

Copyright  
by  
Somudro Gupta  
2011

The Thesis committee for Somudro Gupta  
certifies that this is the approved version of the following thesis:

**Mechatronics of Holonomic Mobile Base for Compliant  
Manipulation**

APPROVED BY

SUPERVISING COMMITTEE:

Supervisor:

---

Luis Sentis

---

Benito Fernández

**Mechatronics of Holonomic Mobile Base for Compliant  
Manipulation**

**by**

**Somudro Gupta, B.S.**

**THESIS**

Presented to the Faculty of the Graduate School of  
The University of Texas at Austin  
in Partial Fulfillment  
of the Requirements  
for the Degree of

**MASTER OF SCIENCE IN ENGINEERING**

The University of Texas at Austin  
December 2011

To our future robot overlords.

## Acknowledgments

I would like to thank my advisor, Luis Sentis, for his support and guidance. His passion for robotics drove me to pursue the research described in this thesis. I also thank Benito Fernández for mentoring and working with me throughout my time at UT, and for serving as my second reader.

My primary collaborators on the Trikey project have been Pius Wong and Frank Lima, and I am grateful to them for their efforts and their company. I must also acknowledge Nick Paine and Josh Petersen, who have contributed significantly to bringing the base to where it is today, and who have answered many of my hardware and software questions. My other HCRL labmates, including Matt Gonzales, Sehoon Oh, Mike Slovich, and Chris Slaughter have all also helped out in one way or another.

I thank Lonny Stern for organizing RoboTech Velocity Prep, and the Del Valle High School students who participated in the program and helped build and name the first prototype of Trikey. I still think the name should have been "Omnilicious," but majority rules.

I acknowledge Meka Robotics for building Trikey's electronics, and I thank everyone who helped host Luis and I during our visit. Robby Kelbley and Benjamin Valenti, especially, have been incredibly patient and competent with debugging our software and hardware issues.

Finally, I am grateful to all of my classmates and friends at UT who have enriched my experience here, and to my parents and sister for their love and support.

# **Mechatronics of Holonomic Mobile Base for Compliant Manipulation**

Somudro Gupta, M.S.E.

The University of Texas at Austin, 2011

Supervisor: Luis Sentis

In order to operate safely and naturally in human-centered environments, robots need to respond compliantly to force and contact interactions. While advanced robotic torsos and arms have been built that successfully achieve this, a somewhat neglected research area is the construction of compliant wheeled mobile bases. This thesis describes the mechatronics behind Trikey, a holonomic wheeled mobile base employing torque sensing at each of its three omni wheels so that it can detect and respond gracefully to force interactions. Trikey's mechanical design, kinematic and dynamic models, and control architecture are described, as well as simple experiments demonstrating compliant control. Trikey is designed to support a force-controlled humanoid upper body, and eventually, the two will be controlled together using whole-body control algorithms that utilize the external and internal dynamics of the entire system.

# Table of Contents

<b>Acknowledgments</b>	<b>v</b>
<b>Abstract</b>	<b>vi</b>
<b>List of Tables</b>	<b>ix</b>
<b>List of Figures</b>	<b>x</b>
<b>Chapter 1. Introduction</b>	<b>1</b>
1.1 Context . . . . .	1
1.2 Trikey and Dreamer . . . . .	2
1.3 Background Review . . . . .	3
1.3.1 Omnidirectional Wheeled Robots . . . . .	4
1.3.2 Platforms for Compliant Mobile Manipulation . . . . .	9
<b>Chapter 2. Design</b>	<b>13</b>
2.1 Objectives . . . . .	13
2.2 Design Evolution . . . . .	14
2.2.1 Trikey 1 . . . . .	14
2.2.2 Trikey 2 . . . . .	16
2.2.3 Trikey 3 . . . . .	19
2.2.4 Trikey 4 . . . . .	20
2.3 Design Calculations . . . . .	22
2.3.1 Torque . . . . .	22
2.3.2 Velocity . . . . .	24
2.3.3 Power . . . . .	25
2.3.4 Torque Sensitivity . . . . .	26
2.4 Component Selection . . . . .	27
2.4.1 Wheels . . . . .	27
2.4.2 Motors & Gearboxes . . . . .	29
2.4.3 Torque sensors . . . . .	32
2.4.4 Torque limiters . . . . .	33
2.4.5 Couplings . . . . .	33

<b>Chapter 3. Modeling</b>	<b>35</b>
3.1 Kinematics . . . . .	35
3.2 Dynamics . . . . .	38
<b>Chapter 4. Control</b>	<b>41</b>
4.1 Version 1: HCRL-MC/Ubuntu RTAI . . . . .	41
4.1.1 Hardware . . . . .	42
4.1.2 Software . . . . .	42
4.2 Version 2: M3/WBC control . . . . .	47
4.2.1 Hardware . . . . .	47
4.2.2 Software . . . . .	49
<b>Chapter 5. Conclusions &amp; Future Work</b>	<b>52</b>
5.1 Summary of thesis . . . . .	52
5.2 Future work . . . . .	53
5.2.1 Control . . . . .	53
5.2.2 Design . . . . .	54
<b>Appendices</b>	<b>55</b>
<b>Appendix A. Operating Instructions</b>	<b>56</b>
<b>Appendix B. Wiring Information</b>	<b>58</b>
B.1 Motor Wiring . . . . .	62
B.2 Torque Sensor Wiring . . . . .	64
B.3 Encoder Wiring . . . . .	65
B.4 AHRS Wiring . . . . .	67
<b>Appendix C. Component Specifications</b>	<b>69</b>
<b>Bibliography</b>	<b>79</b>

## List of Tables

2.1	Design decision matrix . . . . .	16
2.2	Motor + Gearbox, v1 . . . . .	31
2.3	Motor + Gearbox, v2 . . . . .	32
B.1	Connectors for electronics . . . . .	58
B.2	Recommended crimp tools . . . . .	58
B.3	Pinout for JST connector for torque sensor . . . . .	64
B.4	Pinout for circular connector for torque sensor . . . . .	64
B.5	Pinout for JST connector for encoder . . . . .	65
B.6	Pinout for CON-FC5 connector for encoder . . . . .	65
B.7	Pinout for JST connector for AHRS . . . . .	67
B.8	Pinout for 5x2 pin connector for AHRS . . . . .	67
C.1	Major component list . . . . .	69

# List of Figures

1.1	Trikey and Dreamer	3
1.2	Platforms for compliant mobile manipulation	10
2.1	FEA of Trikey base plate	18
2.2	Trikey 2 and power/sensing module	19
2.3	Trikey 3	20
2.4	Trikey 4	21
2.5	Joint torques for Cartesian force of $F_x = 70$ N applied by base	23
2.6	Joint angular velocities for Cartesian velocity $v_x = 1$ m/s of base	25
3.1	Trikey kinematics	36
3.2	Trikey dynamics	39
4.1	HCRL-MC	43
4.2	Daisy-chaining multiple HCRL-MCs	44
4.3	Architecture of custom control software in RTAI	46
4.4	Current control of wheel	47
4.5	Whole-body control architecture	50
B.1	System wiring overview	59
B.2	ELMO motor controller wiring	60
B.3	Pin order and connection information for 5-position JST connector	61
B.4	Motor winding wiring	62
B.5	Hall sensor wiring	63
B.6	Pin order and connection information for CON-FC5 connector	66
B.7	Pin order and connection information for AHRS 5x2 pin connector	68
C.1	Motor datasheet	70
C.2	Gearbox datasheet	71
C.3	Coupling datasheet	72
C.4	Torque sensor datasheet	73
C.5	Torque sensor op-amp circuit on M3_LOADX3 board	74
C.6	Torque limiter datasheet	75

C.7	Omni wheel specifications	76
C.8	AHRS datasheet	77
C.9	AHRS mounting information	78

# Chapter 1

## Introduction

### 1.1 Context

When industrial robots first started appearing in factories around 1960, they were used to release humans from performing dangerous or harmful manufacturing tasks [13]. As such, there was always a degree of separation between robots and humans. Robotics research focused on improving the speed and precision of robotic manipulators, and because designers could reasonably assume that humans would stay away from robots, safety was not as much of a concern. In recent years, demand for robots has evolved beyond their original industrial applications to more service-oriented roles that involve being in close contact with people. As a result, designers in the emerging field of human-centered robotics must ensure that robots can interact safely and naturally with humans, while still meeting the performance requirements of the tasks assigned to them [47].

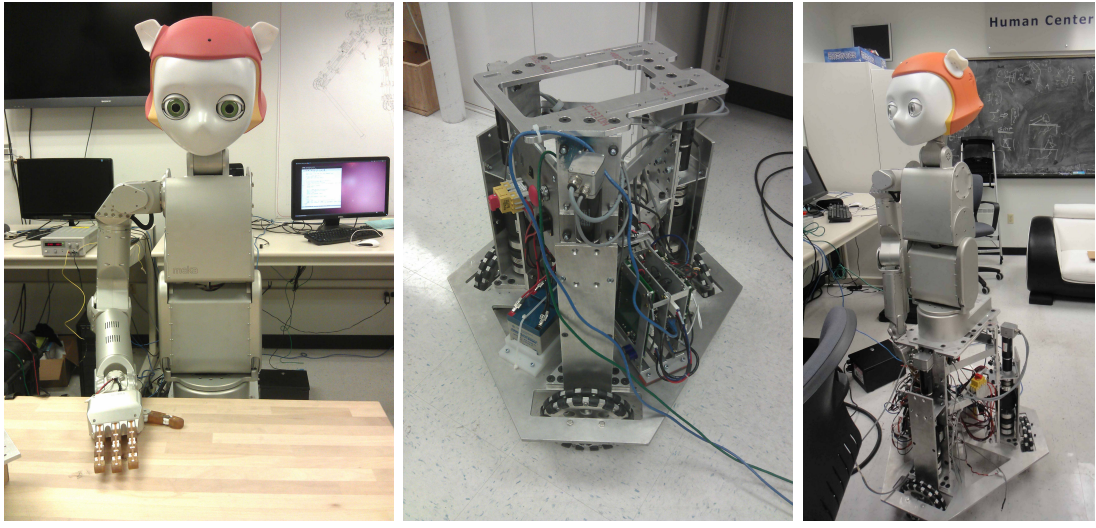
One of the challenges of human-centered robotics is the design and construction of mechatronic devices that can respond to force and contact interactions. While stiff position-control approaches work well for industrial manipulators, they are unsafe for uncertain, human-centered environments where robots must be able to handle collisions gracefully; therefore, force or torque control must be used. Joint torque control [39] and series elastic actuators (SEAs) [45] have been used to build hardware that can be force-controlled and respond compliantly and safely in human-centered environments; examples include the humanoids Justin [6] and Domo [9].

In recent years, many of the advancements in compliant manipulation have focused on humanoid arms and torsos. A somewhat neglected research area is the construction of compliant wheeled mobile bases; most existing bases, even if they support force-controlled upper bodies, are themselves position and velocity controlled [6, 18]. This is somewhat limiting, because colliding with a position controlled base is potentially just as dangerous as colliding with a position controlled manipulator. Ideally, the entire robotic system should be force-controlled if it is operating around humans.

## 1.2 Trikey and Dreamer

In this thesis, we describe the design and development Trikey, a torque-controlled holonomic mobile base for the humanoid upper body Dreamer. Dreamer, produced by Meka Robotics for the Human-Centered Robotics Lab (HCRL), is a humanoid upper body utilizing series elastic actuation in its torso, arm, and hand for safe, compliant force-control. Combining a torque-controlled base with a force-controlled upper body means that the entire robotic system is safe and compliant. In addition, it makes it possible to implement and test control algorithms that utilize the whole-body internal and external dynamics of the system [32]. Successfully doing so could lead to a robot whose abilities to execute complex human-centered tasks in a safe and effective manner will surpass those of existing robots.

Robots are complex machines, and building Trikey has been a significant undertaking. Challenges have included mechanical design of the frame and powertrain, integration of the electronics and power systems, development of the control architecture, and writing control software. Additionally, Trikey began as an educational project, imposing cost and time constraints that had a significant impact on design



(a) Dreamer upper-body

(b) Trikey mobile base

(c) Together

Figure 1.1: Trikey and Dreamer

decisions. This thesis is largely a practical work, describing in detail how to build functional, advanced mechatronic devices amid the constraints imposed by the real world. One of our aims is that others reading this be able to use the information presented here when building their own robots and similar devices.

### 1.3 Background Review

In this section, we first provide an overview of wheeled mobile robots (WMRs) in general, categorized by the type of wheels they use. Similar and extensive overviews are found in [10, 14, 42]. We then present more detail about a few recent platforms for mobile manipulation that have similar objectives to Trikey’s.

### 1.3.1 Omnidirectional Wheeled Robots

#### Holonomic vs. Nonholonomic

In classical mechanics, a system is said to be holonomic if the number of generalized coordinates equals the number of degrees of freedom. A system is said to be nonholonomic if it has fewer degrees of freedom than generalized coordinates [44]. For example, a disc that is constrained to roll on a plane without slipping is a nonholonomic system.

In the field of mobile robotics, a WMR is typically classified as holonomic or nonholonomic based on the kinematic equations describing the abstract robot, even if, strictly speaking, the configuration of its internal components makes it a nonholonomic system according to the classical definition [14, 41]. In this thesis, we adopt the robotics definition of holonomicity.

Holonomic robots have the same number of degrees of freedom as the environment in which they operate. A holonomic ground vehicle in the  $xy$  plane can instantaneously accelerate in the  $x$ ,  $y$ , or  $\theta$  directions. The advantage is that path planning is far easier, and reactive mobile behaviors are readily implemented [14]. For this reason, one of the initial design decisions for our mobile base was that it be holonomic.

A nonholonomic ground vehicle only has a maximum of two degrees of freedom. An example is an automobile, which can be accelerated and steered but cannot translate or rotate in an arbitrary direction. This makes behaviors such as parallel parking or turning in the road difficult, which are non-issues for holonomic vehicles.

Holonomic WMRs have been studied for many years, and some have very innovative designs. The following is an overview of various design options for holonomic mobile robots. Designs that can be considered omnidirectional, but not truly

holonomic based on our definition, are also discussed.

## Omni Wheels

An omni wheel is similar to a conventional rolling wheel, with the addition of smaller rollers along its circumference. The rollers allow the omni wheel to translate laterally, adding a degree of freedom.

While omni wheels do allow for the construction of fully holonomic vehicles, they possess significant disadvantages. The spaces between the rollers mean that, depending on its orientation, the lateral ground friction of the omni wheel varies, inducing vibration during travel. Omni wheels must be manufactured precisely to minimize friction in the rollers when there is a heavy payload. Also, the diameters of the rollers are necessarily smaller than that of the wheel as a whole, making object traversal difficult in the lateral direction.

To overcome the vibration induced by the spaces between the rollers, a double omni wheel possesses a second set of rollers offset from the first. This configuration guarantees that at least one roller always makes full contact with the ground. However, this induces a new type of vibration due to discrete jumps in rotational speed between the rollers.

Numerous WMRs that utilize omni wheels have been built. A common “kiwi” configuration employs three omni wheels spaced  $120^\circ$  apart. One example is the Axebot, which was built to play in the RoboCup Small Size League; its design is discussed in detail in [8]. The mobile base of the ARMAR-III, a humanoid robot, also uses this configuration [1]. The advantages of the kiwi configuration, compared to using four or more wheels, include ease of control; the wheels are more likely to stay in contact with the ground, and there are no redundant DOFs (Degrees of Freedom)

to deal with. Using at least one less motor, gearbox, wheel, motor controller, etc. is also a simpler design with fewer points of failure.

A variation of the traditional omni wheel has the axes of rotation of the rollers offset by  $45^\circ$  (or potentially some other angle) instead of lying along the sagittal plane. Invented by Bengt Ilon of the Swedish company Mecanum AB, this is known as a Mecanum or Swedish wheel. Swedish wheels are typically used in a four wheel configuration on a more conventional rectangular vehicle chassis; this provides greater stability compared to the kiwi configuration and allows engineers to design with more convenient  $90^\circ$  angles. This arrangement is common on holonomic forklifts and industrial manipulators; one example is the KUKA youBot [2]. Unfortunately, Swedish wheels have the same vibration and terrain traversal problems as other omni wheels.

Researchers have developed innovative designs to try to overcome the disadvantages of omni wheels. Song and Byun developed the CAW (Continuous Alternate Wheel), which by utilizing alternating large and small rollers around the wheel, largely eliminates vibration while maximizing passive roller diameter [3]. The same researchers built the OMR-SOW (Omnidirectional Mobile Robot with Steerable Omnidirectional Wheels), which has four steerable omnidirectional wheels in an X-shaped configuration. The steering mechanism alters the robot's footprint and effectively acts as a CVT (Continuously Variable Transmission), enabling higher efficiencies and eliminating the redundant DOF problem that normally exists with four wheels in that configuration [35]. Others have even used omni wheels to build holonomic WMRs that can traverse rough terrain. Chen et al. utilized the “crawler-roller running mechanism” in their Off-road Omni-directional Mobile Robot (OOMR), which can handle rough terrain in any direction [4], while Chugo et al. built an omnidirectional

mobile robot that can climb steps in a single direction [5].

## Ball Drive

A rolling sphere is perhaps the most intuitive holonomic ground vehicle that exists; the difficulty, of course, is in powering and controlling it in a useful way. West and Asada developed a class of ball wheel mechanisms that utilize only rollers (avoiding spherical bearings, which can be difficult to lubricate and seal), and they built a holonomic WMR using three ball wheels that allow smooth motion and precise dead reckoning [41]. More recently, Lauwers et al. developed the Ballbot, which drives a single ball using a powered version of the same mechanism that is inside a ball mouse [25]. Though the early version of the Ballbot could only translate and not arbitrarily rotate about the vertical axis, an improved version added this capability [29]. Kumagai and Ochiai developed the BallIP (Ball Inverted Pendulum), which is similar to the Ballbot, but uses a simpler design employing three omni wheels to drive its ball [23].

A key characteristic of both the Ballbot and BallIP are that they are dynamically stable, meaning they must actively balance to avoid tipping over. Dynamic stability enables them to have a small footprint, high center of gravity, and natural compliance. Lauwers et al. even argue that statically stable robots are an evolutionary dead-end, and that dynamically stable robots are far more suitable for operation in human environments [26]. Disadvantages of robots with dynamic stability include decreased robustness and potentially increased power usage, as they must consume power even when standing still.

## Spherical Orthogonal Wheels

Spherical orthogonal wheels, proposed by Pin and Killough [31], are somewhat of a cross between omni wheels and ball wheels. They consist of two truncated spheres, each of which can rotate around two axes, placed orthogonal to one another but  $90^\circ$  out of phase. When one sphere loses contact (due to the truncation), the other sphere touches the ground. Compared to omni wheels they have fewer moving parts and potentially smoother drivability, but depending on whether they are used in “longitudinal” or “lateral” configuration, they either suffer from discontinuities in ball speeds, or require precise manufacturing to work properly [28]. Spherical orthogonal wheels were used to build the Stanford Assistant Mobile Manipulator (SAMM) platforms [21]; unfortunately, the SAMMs suffered from large reflected inertias, terrible ground clearance, and instability [14].

## Casters

Thus far we have described several “special” wheel types that can be used for creating holonomic vehicles. Conventional wheels, on their own, possess the nonholonomic constraint of not being able to move laterally. Nonetheless, if a conventional wheel is placed in a three DOF caster mechanism, it can be used to construct a holonomic vehicle. A steered conventional wheel has intersecting steer and roll axes, giving it two DOFs (steering and rolling); offsetting the roll axis so it no longer intersects with the steer axis provides a separate twist axis, and thus an additional DOF.

Casters are commonly used on passive vehicles such as office chairs and shopping carts, but the challenges of powering and controlling them were not tackled until relatively recently; Wada and Mori built a WMR using powered casters in 1996 [40].

Holmberg and Khatib developed the Nomad XR4000 PCV (Powered Caster Vehicle), which achieved smooth, dynamically controlled holonomic motion [15]. A substantial advantage of casters over other holonomic mechanisms is that they can use readily available pneumatic tires, which provide much smoother motion and better object traversal, among other advantages, compared to omni wheels and other holonomic counterparts [14].

A disadvantage of casters is the presence of wheel scrubbing when the wheel is twisted about the vertical axis; this can increase tire wear and power consumption, especially with a heavy vehicle or when operating in rough terrain [46]. To counter this, Yu et al. developed the Active Split Offset Castor (ASOC), which reduces scrubbing by placing two wheels on a caster instead of one [46]. Recently, Ishigama et al. built and tested a holonomic mobile robot employing ASOCs to handle rough outdoor terrain [17].

### 1.3.2 Platforms for Compliant Mobile Manipulation

Now that we have reviewed the various types of holonomic WMRs, we turn our attention to a few specific WMRs that were built with objectives overlapping our own - namely, to be used for force-controlled compliant manipulation.

#### Nomad XR4000

The Nomad XR4000, developed by Holmberg and Khatib [14, 15], improved upon existing holonomic platforms both in terms of design and control. As discussed in 1.3.1, using powered casters provides advantages in motion quality, ruggedness, and controllability over designs employing special wheels. Control of powered casters is difficult because there is no unique mapping between joint positions and robot positions, and there is potential for actuator conflict; to tackle this problem, Holmberg

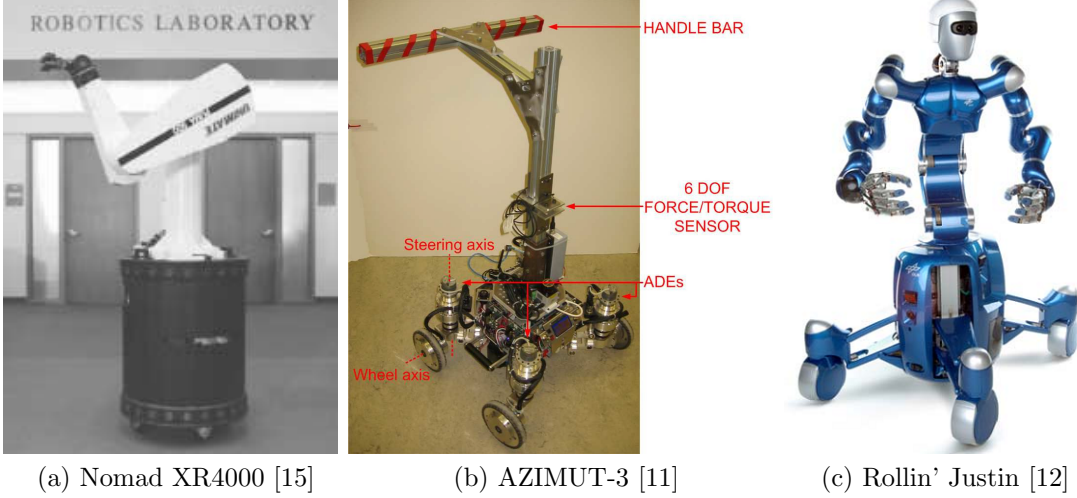


Figure 1.2: Platforms for compliant mobile manipulation

and Khatib model the PCV as a collection of open-chain manipulators to derive its dynamics, and they utilize operational space control [22] to control end effector forces and velocities. To resolve the extra DOFs from using four casters, the contact forces at each wheel are minimized, reducing slip and improving odometry. When a PUMA 560 arm is mounted on the Nomad, dynamic effects can be compensated for, improving mobile manipulation.

A drawback to the Nomad is that there are no torque sensors to measure torque directly, so current control of the motors must be used instead. Current, though roughly proportional to torque in DC motor, is a noisier signal. Furthermore, the torque lost to frictional effects in the drivetrain (after the motor) cannot be measured. The PUMA 560 is also unsafe and outdated compared to current manipulators. Nonetheless, the design and control strategies used are useful in designing safer, more compliant systems.

## AZIMUT-3

The AZIMUT-3, developed by Frémy et al. [11], is a force-guided WMR. Force-guided WMRs such as the CMU Robotic Walker [27] and SmartWalker [36] are designed to be used as a walking platform to assist the elderly or disabled. Typically, the user for such a robot will interact with it haptically via a six DOF force/torque sensor embedded in the handlebar, whose signals are converted to velocity commands; the platform is subsequently velocity controlled in the direction the user wants to walk in [27, 36].

The problem with such an approach is that it 1) requires an expensive and fragile six DOF load cell, and 2) user forces are only sensed at the handlebar, meaning collisions are still not handled gracefully during velocity control; this necessitates additional perception and sensing to avoid collisions. The AZIMUT-3 uses a different approach, utilizing differential elastic actuators (DEAs) [24] to sense forces at the wheels directly while handling collisions safely and compliantly. DEAs offer similar force-control advantages to SEAs, but can allow for a more compact and simpler design for rotational actuators such as the ones in the AZIMUT-3.

A disadvantage of the AZIMUT-3 is that it is not quite holonomic, though it is close to being so. For the purpose it was built for this is not a big problem, but for our objective of supporting a humanoid torso, this aspect of its design would be more of a hindrance.

## Rollin' Justin

Rollin' Justin [12] is the embodiment of DLR's humanoid Justin atop a wheeled mobile base. The base has very similar objectives to ours; Justin, an advanced humanoid upper body utilizing torque sensors in its joints for compliant manipulation,

was built first, and the base was designed afterward to provide it mobility in human-centered environments. The base has a unique design utilizing four independently actuated wheels in a variable footprint mechanism; this allows Justin to maintain stability when manipulating high loads and/or moving at high speeds, and also to fit through narrow passages and doorways. The torso, together with the base, can implement whole-body torque-controlled maneuvers for compliant mobile manipulation [6].

Though sophisticated, the design of the base has several drawbacks. Like most other similar platforms, it is controlled kinematically but not dynamically. To prevent collisions, the base contains time-of-flight cameras that are used to generate potential fields around the base in the whole-body controller. The base is also nonholonomic, further complicating its control structure [7].

# Chapter 2

## Design

The Trikey project began as part of Skillpoint Alliance’s Robotech Velocity Prep program, whose purpose is to improve science and technology education among high school students by providing them with professional engineering work experience. Fifteen students formed a mock company that was asked to complete a robotics engineering project for a client. In this case, this involved working on a prototype mobile base for HCRL (Human-Centered Robotics Lab) research. After Velocity Prep’s completion, Trikey was successively upgraded to better fulfill the research goals of implementing compliant and whole-body control algorithms.

In this chapter, we first describe Trikey’s design objectives. This follows with a mostly qualitative description of each of Trikey’s design iterations as it progressed from its educational origins to a sophisticated, research-grade robot. Finally, we go into more quantitative detail concerning the design.

### 2.1 Objectives

Trikey’s ultimate objective is to support Dreamer in performing manipulation tasks in human-centered environments. To function in this role, we can summarize the objectives of Trikey’s design via the following requirements:

- It should be holonomic. As defined in 1.3.1, this means it can instantaneously accelerate in the  $x$ ,  $y$ , or  $\theta$  directions

- It should be able to detect and react to an external agent that is pushing on it at any point in its body. The minimum force the base should be able to detect is  $F_e = 5 \text{ N}$ .
- It must be able to safely support the humanoid upper body Dreamer. This means it must be able to support the weight of the upper body, and its actuators must be capable of overcoming the additional inertial and frictional forces that arise from it.
- It should be able to translate in any direction at a velocity of  $1 \text{ m/s}$ , and accelerate at  $1 \text{ m/s}^2$ .
- It must fit through a standard doorway, which in the US is about 32 inches horizontally.
- The combined height of Trikey and Dreamer should be approximately human height, and of course also fit through a standard doorway.

## 2.2 Design Evolution

In this section, we describe each of Trikey's design iterations and explain the general design decisions made for each. In addition to providing an overall understanding of the design, this is meant to provide the reader context for when we later describe the design in more quantitative detail.

### 2.2.1 Trikey 1

The original version of Trikey was the direct result of the Velocity Prep program. The general objectives described in 2.1 were presented to the students involved,

who were tasked with building a basic prototype and progressing as far toward those objectives as possible.

In 1.3 we discussed several design options for holonomic robots. Of these, we presented kiwi drive (three omni wheels, with straight rollers, spaced  $120^\circ$  apart around the base's  $z$ -axis), Mecanum drive (four Mecanum wheels in a rectangular configuration), ball drive, and powered casters as potential options to students and discussed the advantages and disadvantages of each option.

Powered casters were ruled out early on due to their cost and complexity; a prototype would be exceedingly difficult to build within the required time frame and budget. Of the remaining options, kiwi drive was the simplest, and it was decided that the advantages of the other options did not outweigh the disadvantages posed by their increased complexity and cost. Therefore, kiwi drive was selected. Because Velocity Prep took place in a high school with no machine shop, it was also decided that the mechanical structure for the base would initially be made from wood. This reduced cost and complexity and allowed for significantly easier prototyping, with more contributions from the students in the program.

The matrix below outlines the design options initially considered. The advantages and disadvantages are roughly ranked on a five point scale, with five indicating most advantageous (e.g. lowest cost, highest robustness, etc.), and one indicating least advantageous (e.g. longest build-time, poorest motion quality, etc.). We can derive a utility function as a weighted sum of each factor that is important: cost, build-time, robustness, and motion quality (i.e. lack of vibration). The constraints of the Velocity Prep program lead to cost and build-time being weighted more highly, yielding the following function,

	cost	build-time	robustness	motion quality	$u$
kiwi drive	5	4	4	3	4.1
Mecanum drive	3	4	4	3	3.5
ball drive	2	2	2	4	2.4
powered casters	1	1	2	5	2

Table 2.1: Design decision matrix

$$u = 0.3c + 0.3b + 0.2r + 0.2m \quad (2.1)$$

where  $c$  is cost,  $b$  is build-time,  $r$  is robustness, and  $m$  is motion quality, all on a five point scale. The results point to kiwi drive as the winner, given the relevant constraints.

By the end of Velocity Prep, a basic mechanical structure including omni wheels was completed. Though students learned about electronics, control, programming, and component selection, the full integration of motors, gears, and electronics with the mechanical structure was not completed until the next design iteration. Temporary components, consisting of an Arduino sending control signals to brushed DC motors connected directly to the omni wheels, did allow the robot to move for demonstration purposes.<sup>1</sup>

### 2.2.2 Trikey 2

Though constructing the Velocity Prep version of Trikey was valuable as an educational experience and proof-of-concept, the wooden structure was not suitable for long-term research purposes. It was therefore decided to progress to a more robust aluminum frame. Furthermore, the BLDC motors and gearboxes that had

---

<sup>1</sup>Credit is due to collaborator Frank Lima and the students of Velocity Prep for their significant contributions to building Trikey 1.

been selected needed to be integrated into the mechanical structure for torque control and whole-body control to be possible.

To sense torque, designing a custom torque sensor was initially considered. This would consist of a rotational spring in series with the wheel and connected to a pair of encoders that would calculate spring deflection. Acting as a type of series elastic actuator (SEA) in conjunction with a motor and gearbox, this would add compliance to the wheel and enhance torque control, while also avoiding the cost of purchasing expensive load cells. However, this idea was eventually abandoned in favor of purchasing torque sensors that utilize strain gauges to measure torque. The analysis that led to this decision is explained later in this thesis.

In order to fit all of the required actuator and sensor components for each wheel into a robot that would be able to fit through a standard doorway, we adopted a design that places the components in series vertically. A set of miter gears (bevel gears at  $90^\circ$  with a 1:1 gear ratio) at the final output shaft of each wheel translates rotational motion of the vertical axis to the horizontal axis of the wheel. We refer to each set of actuators and sensors that work to power and sense the motion of a wheel as a *power/sensing module*.

A single aluminum plate at the bottom holds the three power/sensing modules. This plate has a maximum width of 30", which can allow Trikey to fit through a standard 32" US doorway, while maximizing static stability and room for electronics and batteries. The cutouts in the plate minimize weight, and FEA was performed to ensure the plate would remain rigid under a load of 500 N at each power/sensing module interface, which would be enough to support the upper body and any batteries and electronics placed inside the base.

The final constructed base is shown in Figure 2.2, along with a closeup of a

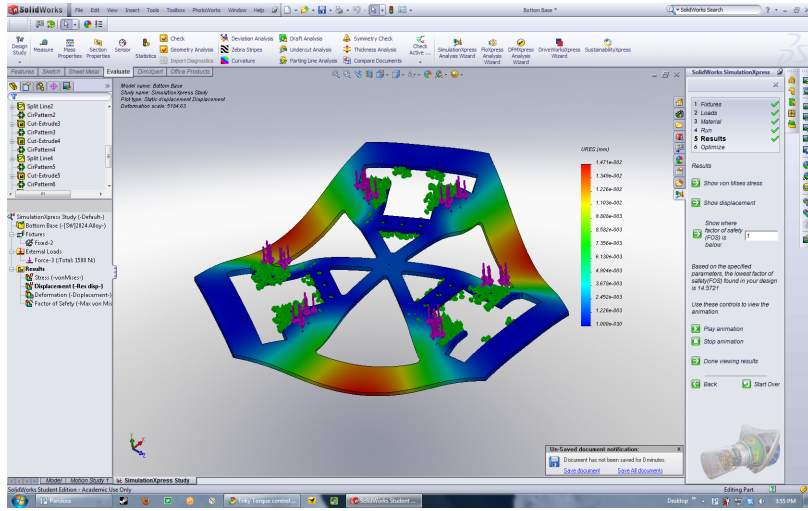


Figure 2.1: Finite element analysis of base plate. Maximum deflection is  $1.471 \cdot 10^{-2}$ mm for an applied force of 500 N at each power/sensing module interface.

single power/sensing module for a wheel. The components, from top to bottom, are the following: BLDC motor, 48:1 planetary gearbox, encoder, rigid shaft coupling, torque sensor, clutch, miter gears (top miter gear not visible), and omni wheel (to the left). The shaft coupling acts as a power interface between the smaller diameter shaft of the gearbox and encoder output and the larger diameter torque sensor shaft. The clutch is set to disengage at an output torque threshold of 60 Nm in order to protect the torque sensor; if the applied torque drops below the threshold the clutch automatically re-engages.

A key element of the design is that the torque sensor is located as close as possible to the wheel. The only components between the torque sensor and wheel are the clutch and miter gears, with the efficiency of the clutch being close to 100%, while the efficiency of miter gears is typically between 80% and 90% [20]. This means that wheel torque can be measured and controlled accurately in a feedback control loop, without needing to model the losses in the motor and gearbox. This is not the

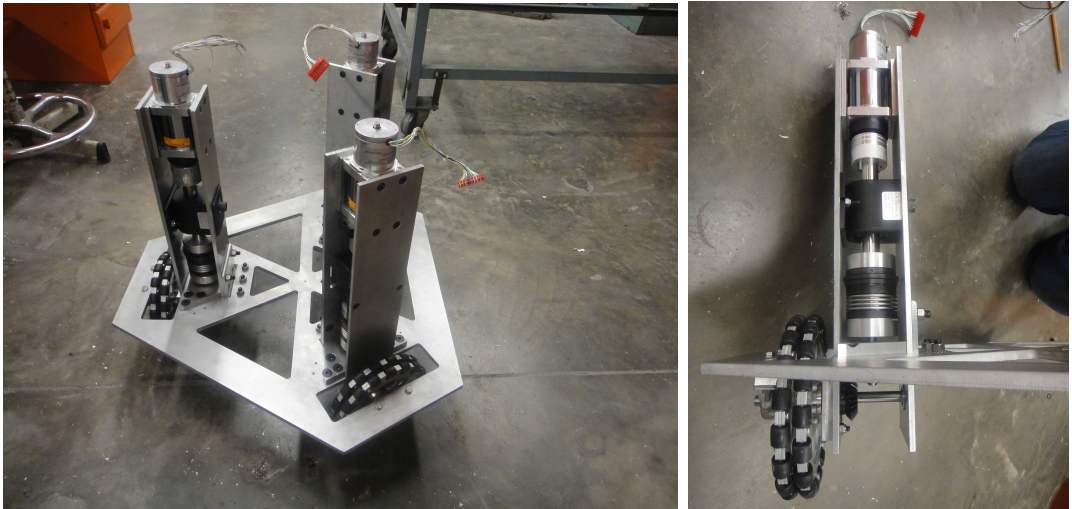


Figure 2.2: **Left:** Final constructed version of Trikey 2. **Right:** Closeup of power/sensing module. The components, from top to bottom, are the following: BLDC motor, 48:1 planetary gearbox, encoder, rigid shaft coupling, torque sensor, clutch, miter gears (top miter gear not visible), and omni wheel (to the left).

case if torque is estimated simply by measuring motor current.<sup>2</sup>

### 2.2.3 Trikey 3

While the aluminum structure and vertical module design of Trikey represented a major step forward, the design contained several limitations. Most significantly, the planetary gearboxes had much more friction than initially anticipated. The rigid shaft coupling in each power/sensing module also did not allow for misalignment in the gearbox output shaft, thereby exerting forces on the planetary gear stages in the gearbox and increasing friction even more. Consequently, the wheels could not be smoothly and reliably turned, and the gearboxes could not be backdriven, making torque control unachievable.

To rectify these problems, the motors, gearboxes, and couplings were replaced.

---

<sup>2</sup>Credit is due to collaborator Frank Lima for doing the CAD and machining of Trikey 2's frame.

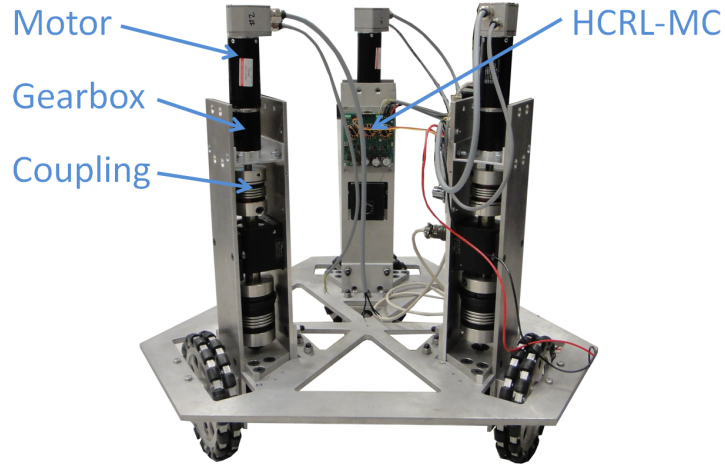


Figure 2.3: Trikey 3. The new components, compared to Trikey 2, are highlighted.

Higher precision gearboxes with a lower gear reduction ensured increased backdrivability and lower friction. To compensate for the lower gear reduction, more powerful motors that generated more torque were chosen. Finally, high quality flexible shaft couplings allowed for misalignment and ensured smooth rotational motion.

The new power/sensing module design is visible in Figure 2.4. When paired with the HCRL-MC motor control boards and Ubuntu RTAI control architecture, successful current control of the wheels was achieved.<sup>3</sup>

#### 2.2.4 Trikey 4

Trikey 3 was a functional torque controlled base. However, it needed to be tethered, both for computation and power purposes. The miter gears were problematic and would frequently misalign after motion took place, increasing backlash. The

---

<sup>3</sup>Credit is due to HCRL students Pius Wong and Nicholas Paine for their contributions to Trikey 3. Pius calibrated the torque sensors and helped with machining, and Nick designed the HCRL-MC board and helped significantly with developing Trikey 3's control architecture in RTAI.

base also did not contain mechanical structures for holding the Dreamer humanoid torso, which would be needed to apply whole-body control to a full humanoid system. Trikey 4 saw the addition of these features. In order to facilitate ease of long-term maintenance, the custom control architecture utilizing the HCRL-MC and Ubuntu with RTAI was replaced with a power system, control electronics and M3 control software designed by Meka Robotics. Concurrently, mechanical structures to hold these systems were designed and built. In addition, spacers were added to the axles holding the miter gears, greatly improving durability.<sup>4</sup>

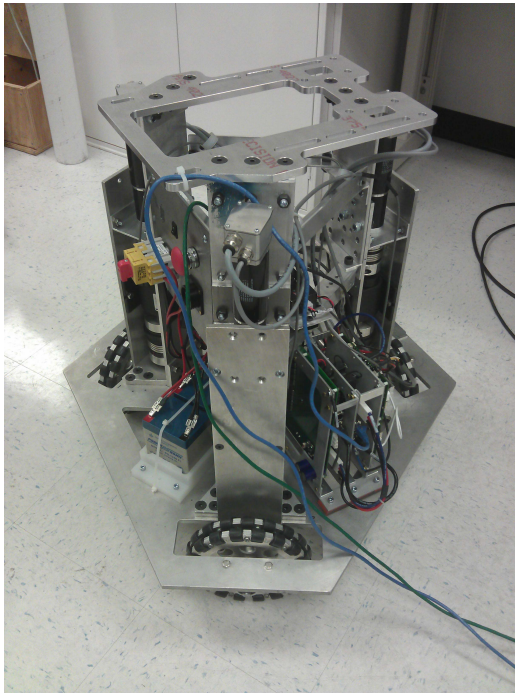


Figure 2.4: Trikey 4. The new components, compared to Trikey 3, are the electronics (bottom right), batteries (bottom left), user panel with switches and outlet for tethered power (top left), and structures for holding Dreamer (top, center).

---

<sup>4</sup>Credit is due to HCRL student Pius Wong for designing and building the new mechanical structures in Trikey 4.

## 2.3 Design Calculations

While in the previous section we discussed the design iterations of Trikey qualitatively, we now go into more quantitative detail on the calculations performed to design and select components of the base. We will utilize the models described in Chapter 3 to aid us in performing calculations.

### 2.3.1 Torque

In Chapter 3 we derive the dynamic model for Trikey. In that chapter, the relationship between joint (actuated wheel) torques and Cartesian forces and moments applied by the mobile base is derived and given by Equation 3.17. In this section we use this equation to derive the torque requirements for the motors, gearboxes, and other components we will use in our design.

Note that, as demonstrated by Equation 3.14, for a given wheel traction force  $F_i$ , the torque that needs to be supplied to the wheel is proportional to the wheel radius. Thus, wheel radius is essential to motor and gearbox selection; doubling the wheel radius, for example, doubles the required torque output from the gearbox, resulting in a higher gear reduction or more powerful motor that needs to be selected. In the case of the present analysis, however, price, weight, and availability constraints led to few choices for selecting omni wheels. Thus, a wheel was already chosen before motors and gearboxes were selected, and we use its given radius of  $r_w = 0.1016 \text{ m}$  (4") for the remainder of our analysis.

In order for responsive torque control to be possible, we specify that motors and gearboxes should be selected such that an acceleration of at least  $1 \text{ m/s}^2$  is achievable in any direction. First, using Equation 3.17, we write a Matlab function that computes joint torques based on global Cartesian forces and moments and the present

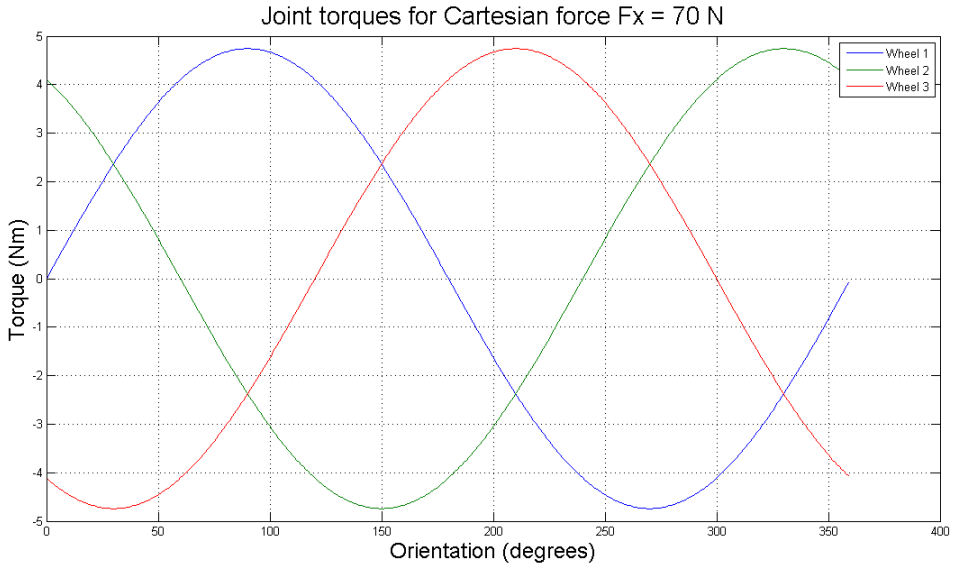


Figure 2.5: Joint torques for Cartesian force of  $F_x = 70$  N applied by base

orientation of the base ( $\theta$  in Equation 3.17, and as depicted in Figure 3.2). A mass of 70 kg is assumed, which is a high estimate of the total mass of the base, electronics, batteries, and humanoid torso combined. We then write a script that executes the function with an input force of 70 N*i* (which, given our mass estimate, is equivalent to an acceleration of 1 m/s<sup>2</sup> in the *x* direction, *i* being the unit vector in the *x* direction) for orientation angles of 0-359°, computed every 1°. The resulting joint torques are plotted in Figure 2.5.

Maximum joint torque is achieved when the wheel axis is perpendicular to the direction of the total applied force (while the remaining two joints (wheels) have equal but lesser torques in the opposite direction). We can see that the orientation angle of the maximum torque for wheel *i* is given by the following:

$$\text{At max } \tau_i, \theta_i = \frac{\pi}{2} + \alpha_i \quad (2.2)$$

This yields values of 90°, 210°, and 330°. The maximum torque in this case, for any

wheel, is 4.74 Nm. We will keep this value in mind during component selection.

### 2.3.2 Velocity

We now repeat the above analysis, but for velocities instead of forces and torques. In Chapter 3, the relationship between joint angular velocities (i.e. actuated wheel angular velocities) and the Cartesian velocity of the base is given by Equation 3.8. Again, because we have a wheel selected already, we assume a given wheel radius of  $r_w = 0.1016\text{m}$ ; we use this value to convert linear actuated wheel velocities to joint angular velocities, as given by Equation 3.6.

We specify that for useful movements and tasks to be possible, the base should be able to move with a velocity of at least  $1\text{ m/s}$  in any direction. To determine joint angular velocities seen by the wheels, we write a Matlab function that computes joint angular velocities based on global Cartesian velocities and the present orientation of the base ( $\theta$  in Equation 3.8, and as depicted in Figure 3.1). We then write a script that executes the function with an input velocity of  $1\text{ m/s}\mathbf{i}$  for orientation angles of  $0\text{--}359^\circ$ , computed every  $1^\circ$ . The resulting joint angular velocities are plotted in Figure 2.6.

As with torque, maximum joint angular velocity of each wheel occurs when the axis of the wheel is perpendicular to the direction of the total Cartesian velocity of the base. The orientation angle of the maximum joint angular velocity for wheel  $i$  is given by the following:

$$\text{At max } \phi_i, \theta_i = \frac{\pi}{2} + \alpha_i \quad (2.3)$$

which, being identical to Equation 2.2, yields the same angles of  $90^\circ$ ,  $210^\circ$ , and  $330^\circ$ . The maximum joint angular velocity, in this case, is  $9.84\text{ rad/s}$ , or  $94.0\text{ rpm}$ . We will

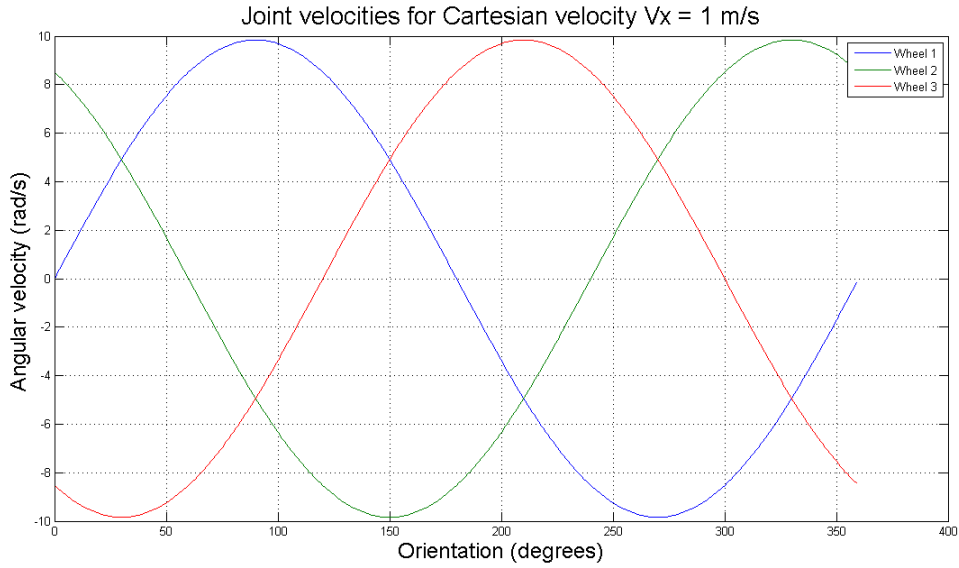


Figure 2.6: Joint angular velocities for Cartesian velocity  $v_x = 1 \text{ m/s}$  of base

keep this value in mind during component selection.

### 2.3.3 Power

The power required to drive each wheel can be calculated by multiplying joint torque with joint angular velocity:

$$P_i = \tau_i \dot{\phi}_i \quad (2.4)$$

Thus, to calculate motor power requirements, we should know how much torque is required to spin the wheels at different angular velocities. Exact numbers are difficult, because in practice much of this torque comes from friction, and it is difficult to estimate friction accurately without measuring it on actual hardware. For a ballpark estimate, we can specify that the base should be able to exert the maximum torque calculated earlier, while moving at the maximum angular velocity:

$$P_{i,req} = \tau_{i,max} \dot{\phi}_{i,max} \quad (2.5)$$

This yields a required power of  $4.74 \text{ Nm} \times 9.84 \text{ rad/s} = 46.6 \text{ W}$  delivered at each wheel.

### 2.3.4 Torque Sensitivity

Recently there have been efforts to improve upon traditional strain gauge torque sensors, which tend to be fragile and expensive. Vischer and Khatib developed torque sensors that utilize contactless inductive transducers [39], while Shams et al. adopted an optical approach utilizing a photo-interrupter to measure torque [34].

Rather than purchasing load cells, we explored building a custom torque sensor that would be compliant and measure deflection optically. This sensor would consist of a rotational spring in series with the wheel and connected to a pair of encoders (one on each end of the spring) that would calculate spring deflection. The purpose of such a sensor is to detect not only the torque applied to the wheel by the motor, but also reaction torques that arise due to external forces that are applied to the base. We can specify a minimum external wheel force the sensor can detect as  $\Delta F_w$ ; this determines the minimum resolution  $\Delta\tau_w$  of the torque sensor via the formula,

$$\Delta\tau_w = r_w \Delta F_w \quad (2.6)$$

where  $r_w$  is the wheel radius. Assuming a linear rotational spring of stiffness  $k$ , the minimum torque induces a change  $\Delta\theta$  calculated by,

$$\Delta\theta = \frac{\Delta\tau_w}{k} \quad (2.7)$$

Assuming SI units for all terms, from 2.6 and 2.7 we can determine the minimum pulses per revolution (PPR)  $p$  for an encoder to detect the minimum resolution wheel torque or force:

$$p = \frac{2\pi k}{\Delta\tau_w} = \frac{2\pi k}{r_w \Delta F_w} \quad (2.8)$$

Once a minimum resolution is decided upon, designing the torque sensor involves a tradeoff between  $p$  and  $k$ . As discussed in [45], a lower stiffness  $k$  in a series elastic actuator decreases control bandwidth while gaining safety (for both the actuator and humans) and more stable force control [9, 45]. Furthermore, in this case, a lower  $k$  decreases  $p$ , which substantially decreases encoder cost. However, it can be difficult to find springs with both low  $k$  and high yield strength [45], and we found the same to be true of rotational elastic couplings. Traditional torque sensors work on the same principle, but intentionally use high torsional stiffness with strain gauges. Consequently, they can be quite expensive and fragile.

## 2.4 Component Selection

Now that we have completed the basic calculations needed to select components in our design, we detail the requirements of each component qualitatively, how each component was selected, and the final specifications of each component. Because cost and availability sometimes acted as significant design constraints as well, these are explained in addition to pure engineering requirements.

### 2.4.1 Wheels

The selection of a wheel was critical to Trikey's design. As demonstrated by Equation 3.14, increasing the wheel radius directly increases the required output

torque. Larger wheels might also be harder to fit within a frame that can fit through a standard doorway. Conversely, wheels that are too small have difficulty in traversing obstacles, and the angular velocities are higher, leading to increased bearing friction torques. Rollers are also critical to wheel selection; the passive rollers must be of sufficient rigidity and quality that they can overcome rolling resistance forces and bearing torques that arise from the weight of the base and upper body. Larger, precision-made rollers can bear more weight.

For Trikey's requirements, wheels with a diameter of approximately 10" were desired. However, most omni wheels currently on the market are either much smaller or larger in diameter. The smaller wheels are typically made of plastic and produced by companies such as Vex or Dagu, who sell them for use in small, educational robotics projects and toys. The larger wheels are designed for industrial use, such as omnidirectional forklifts. These are considerably heavier, larger, and more expensive. Prices and delivery times for industrial omni wheels were out of reach for Trikey's initial budget and time constraints.

We ended up choosing 8" aluminum dual omni wheels made by AndyMark, shown in Figure. AndyMark supplies parts for FIRST robotics competitions, whose robots tends to be larger than toys but below industrial sizes and standards. The dual omni wheels are constructed simply by screwing together two single omni wheels with the rollers offset, resulting in increased roller contact and an increased load capacity up to 100 lbs. Because each omni wheel bears about one-third of the total weight, this means that the base could weigh up to 300 lbs before the omni wheels would be outside their specifications. This is about double its expected actual weight. The cost of each wheel was economical, at \$107 each.

### 2.4.2 Motors & Gearboxes

The motor and gearbox together need to meet the output torque and angular velocity requirements of each wheel. Though they have some separate requirements, selecting them both should be an iterative process that occurs simultaneously.

In order to work with the HCRL-MC torque-control motor control boards that were being designed concurrently, it was decided early on to select brushless DC (BLDC) motors. Though mechanically commutated brushed DC motors are less expensive and much simpler to use than their brushless counterparts, they have more friction and suffer wear over time. AC motors are ubiquitous in the industrial world, but less common in academic robotics research because they are more difficult to control and interface with other hardware.

Backdrivability is an essential requirement for gearboxes in any compliant, human-safe robotic application, including Trikey. As described by [16], backdrivability relates the ease that an actuator can be turned at its output axis in order to move its inner axis components. If less resistance torque is encountered for motion to occur, the actuator can be said to be more backdrivable. Backdrivability can be improved by decreasing the friction and inertia of the gearbox. Because reflected inertia is a function of the square of the gear ratio, changing the gear ratio can have a dramatic effect on backdrivability.

Another requirement for Trikey's gearboxes was that they be low backlash. Though backlash is less of a problem in compliant robotics than industrial robotics, where precise positioning is much more important, it nonetheless reduces controllability and the precision of tasks that can be performed. A popular gearbox option in robotics is the harmonic drive (also known as strain wave gearing), which is characterized by compactness and zero backlash. However, harmonic drives are expensive,

and are not necessarily as backdrivable as more economical and ubiquitous planetary gearboxes. Though having too many stages and gear reductions can be problematic, high quality planetary gearboxes with a lower gear ratio and less than four stages can be easily backdrivable and exhibit low backlash.

## Motor + Gearbox: Version 1

The initial BLDC motors that were chosen for the Trikey project were Moog BN23HP motors. These motors were custom-made for a company that went out of business, and were thus available at a heavily discounted price.<sup>5</sup> Each motor was paired with a P80 3-stage 48:1 planetary gearbox supplied by BaneBots, another company that supplies parts for FIRST competitions. The specifications of the motor/gearbox combination are shown in Table 2.2. The rated mechanical motor power of 86 W is a bit less than double the calculated power requirements of 46.6 W at each wheel, allowing for a 42% power loss through the drivetrain. The high gear ratio leads to an ideal (assuming no losses) output torque of 13 Nm, significantly higher than the 4.74 Nm requirement calculated earlier, while the output speed of  $6.3 \text{ rad/s}$  (at rated motor speed) is less than the calculated requirement of  $9.84 \text{ rad/s}$ . A caveat to the motor specifications, however, is that they assume a nominal voltage of 12 V, while in reality we planned to run the motors at 24 V. Because in a DC motor velocity is roughly proportional to applied voltage and current is proportional to torque, this would generally lead to lower torque and higher velocities than otherwise stated. Nonetheless, we can conclude that this motor/gearbox combination leads to relatively high torque and low speed compared to the requirements described earlier, with adequate power if frictional losses in the drivetrain are not too great.

---

<sup>5</sup>Presumably, ordering the motors did not contribute to the company's downfall.

Rated motor torque	0.28 Nm
Rated motor speed	303 rad/s
Rated motor power	86 W
Gear ratio	48 : 1
Ideal output torque	13 Nm
Estimated output speed	6.3 rad/s

Table 2.2: Motor + Gearbox, v1

### **Motor + Gearbox: Version 2**

As discussed in 2.2.3, the BaneBots gearbox ended up having more friction than was anticipated, leading to greater power loss and insufficient backdrivability. Though better lubrication and a flexible shaft coupling might have reduced friction, it was decided that a new motor/gearbox combination would have a higher probability of succeeding. New motors and gearboxes were purchased from Maxon, a manufacturer of precision motors and gearboxes. The selected motor was the EC-45 24V, 250W, 3-phase BLDC motor, while the selected gearbox was the GP-42-C three-stage planetary ceramic gearbox with a 43:1 reduction ratio.

Specifications of the new motor/gearbox combination are shown in Table 2.3. Note that the output torque takes into account the maximum gearbox efficiency of 72%, specified in the datasheet. Also, operation above nominal values is possible for both torque and speed, and motor electrical power is 250 W with max efficiency of 84%, yielding a maximum actual power of 210 W, which is well above the stated nominal power. Even with these relatively conservative estimates, we can see that, by a wide margin, this motor and gearbox meet the requirements specified earlier.

Nominal motor torque	0.310 Nm
Nominal motor speed	473 rad/s
Nominal motor mechanical power	147 W
Gear ratio	43 : 1
Estimated output torque	9.58 Nm
Estimated output speed	11.0 rad/s

Table 2.3: Motor + Gearbox, v2

#### 2.4.3 Torque sensors

Using Equation 2.8, we attempted to design a compliant torque sensor. For control and protection during collisions, we decided the torque sensor should be able to detect up to 30 Nm of torque. The original specifications stated that Trikey should detect a minimum external force of 5 N. For simplicity, let us assume that this translates to a 2.5 N force at the joint level (on the wheel), or 0.25 Nm of torque on a wheel with radius  $r_w = 0.10$  m. We can now select an appropriate rotational spring of stiffness  $k$  and encoders with PPR (pulses per revolution)  $p$ .

We contacted R+W, a large manufacturer of precision shaft couplings and torque limiters. They recommended either the EK2/60/C elastomer coupling, with torque rating of 20 Nm (peak torque 35 Nm) and approximate torsional rigidity ( $k$ ) of  $1400\text{Nm/rad}$ , or EK2/20/A elastomer coupling, with torque rating of 17 Nm (peak torque 34 Nm) and  $k$  of  $1140\text{Nm/rad}$ . Plugging these values of  $k$  into 2.8, we get  $p = 35,186$  for the former and  $p = 28,651$  for the latter. Even with a very low torque resolution of 0.25 Nm and relatively low torque ratings, these represent high encoder minimum PPRs; though encoders with this resolution do exist, it was decided that the cost of obtaining them would not be justifiable, given the prevalence of less expensive load cells with higher resolution and torque ratings, albeit the lack of rotational compliance.

Replacing the custom-made compliant torque sensor, we decided to buy rotary load cells that measure torque using strain gauges. The torque sensor we selected was the Sensor Developments 01324-052, which can detect up to 56 Nm of torque (and with overload protection of 150% of this value), with a sensitivity of  $0.18 \text{ mV/Nm}$ . This, of course, is the raw signal from the strain gauge, which must then be amplified by the control board.

#### 2.4.4 Torque limiters

Severe, unforeseen collisions of the mobile base could exert very high torques on sensitive, expensive components in the drivetrain, especially the torque sensor and gearbox. To protect these components, it is necessary to utilize torque limiters that disengage the wheel from the rest of the drivetrain once a preset torque limit is reached. The torque limiter should also re-engage once the torque falls back within safe limits.

We selected the adjustable SK2 backlash-free torque limiter from R+W to fulfill these requirements. Originally, we set the SK2s to disengage at 60 Nm to protect the torque sensors, because the original gearboxes were specified to handle up to 115 Nm of torque. The new gearboxes, however, are only specified to tolerate 22 Nm of peak torque, so the limit on the SK2s was lowered. The SK2 also allows up to  $1^\circ$  of angular misalignment, in addition to axial and lateral misalignment.

#### 2.4.5 Couplings

Couplings transfer rotation between discrete shafts while allowing for axial, lateral, and angular misalignment. The original rigid shaft couplings that connected the gearbox output shafts to the torque sensors did not allow for any misalignment, thereby exerting forces on shafts and gears and contributing to increased friction dur-

ing rotation. To correct this, the rigid shaft couplings were replaced by backlash-free BKL30 couplings manufactured by R+W. These allow for 1mm of axial misalignment, 0.2mm of lateral misalignment, and  $1^\circ$  of angular misalignment, with a torque rating of 30 Nm. The result is much smoother rotation.

# Chapter 3

## Modeling

In this chapter we derive the kinematics and dynamics of Trikey. The kinematics and dynamics tell us what the velocities and forces of the individual robot joints are, given global robot velocities and forces that are either specified as control inputs or encountered in the environment. Though others have used various methods to derive the kinematics and dynamics of robots in the same configuration [37, 38], we endeavor to be clearer and go into more depth in our derivations.

### 3.1 Kinematics

Trikey's kinematics are determined by its three omni wheels, which are spaced equally apart around the center of the base. In Figure 3.1, the  $x_r y_r$  frame is located at the center of the base, while  $(x, y, \theta)$  coordinates in the  $xy$  frame define the base's global position and orientation in 2-D space. The location of each omni wheel  $i = \{1, 2, 3\}$  in the local  $x_r y_r$  frame is represented by the polar coordinates  $(R, \alpha_i)$ , with  $R$  representing the distance from the base center to each wheel, and  $\alpha_1 = 0$ ,  $\alpha_2 = 120^\circ$ , and  $\alpha_3 = 240^\circ$ . Each velocity vector  $\mathbf{v}_i$  represents the total velocity of the center of each omni wheel.  $\mathbf{v}_i$  is broken down into orthogonal components  $\mathbf{v}_{i,w}$  and  $\mathbf{v}_{i,r}$ , which represent the actuated wheel linear velocity (proportional to joint angular velocity), and passive roller linear velocity, respectively. Our objective is to find the relationship between the global Cartesian velocity  $(\dot{x}, \dot{y}, \dot{\theta})$  and each actuated wheel velocity  $v_{i,w}$ . From there we can determine joint angular velocities, as well as motor and gearbox

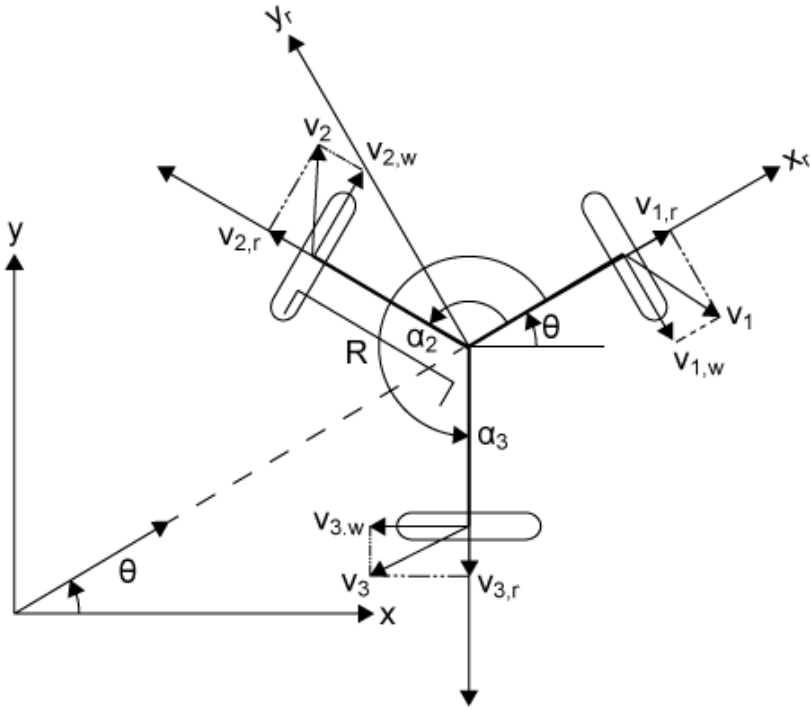


Figure 3.1: Trikey kinematics

local angular velocities.

We know from elementary mechanics that for two points  $A$  and  $B$  on a rigid body, we can find the velocity of  $A$ , given the velocity of  $B$ , via the following:

$$\mathbf{v}_A = \mathbf{v}_B + \boldsymbol{\omega} \times \mathbf{r}_{A/B} \quad (3.1)$$

where  $\mathbf{v}_A$  is the velocity vector of  $A$ ,  $\mathbf{v}_B$  is the velocity vector of  $B$ ,  $\boldsymbol{\omega}$  is the angular velocity vector of the rigid body, and  $\mathbf{r}_{A/B}$  is the position vector from  $B$  to  $A$ . We apply Equation 3.1 to obtain the wheel hub velocity vector  $\mathbf{v}_i$  in terms of the translational and rotational velocity of the base:

$$\mathbf{v}_i = \dot{x}\mathbf{i} + \dot{y}\mathbf{j} + \dot{\theta}\mathbf{k} \times (R \cos(\theta + \alpha_i)\mathbf{i} + R \sin(\theta + \alpha_i)\mathbf{j})$$

where  $\mathbf{i}$ ,  $\mathbf{j}$ , and  $\mathbf{k}$  are unit vectors in the global  $xy$  frame. Simplifying and regrouping, we get:

$$\mathbf{v}_i = (\dot{x} - R\dot{\theta} \sin(\theta + \alpha_i))\mathbf{i} + (\dot{y} + R\dot{\theta} \cos(\theta + \alpha_i))\mathbf{j} \quad (3.2)$$

Assuming no wheel slip, we can obtain the actuated wheel velocity from the vector projection of  $\mathbf{v}_i$  onto the unit vector pointing in the direction of each wheel:

$$v_{i,w} = \mathbf{v}_i \cdot \mathbf{e}_{i,w} \quad (3.3)$$

where

$$\mathbf{e}_{i,w} = \sin(\theta + \alpha_i)\mathbf{i} - \cos(\theta + \alpha_i)\mathbf{j} \quad (3.4)$$

Plugging 3.2 and 3.4 into 3.3 and simplifying, we get the following:

$$v_{i,w} = \dot{x} \sin(\theta + \alpha_i) - \dot{y} \cos(\theta + \alpha_i) - R\dot{\theta} \quad (3.5)$$

We can find the actuated wheel angular velocity  $\dot{\phi}_i$  from the following:

$$\dot{\phi}_i = \frac{v_{i,w}}{r_w} \quad (3.6)$$

where  $r_w$  is the wheel radius. Plugging 3.5 into 3.6 we can convert to the matrix form,

$$\dot{\phi} = \mathbf{J}^{-1}\dot{\mathbf{u}} \quad (3.7)$$

where  $\mathbf{J}^{-1}$  is the inverse Jacobian, which maps joint velocities (in this case, actuated wheel angular velocities) to global Cartesian velocities  $\dot{\mathbf{u}}$ . The result, plugging in values of  $\alpha_i$ , is the following:

$$\begin{bmatrix} \dot{\phi}_1 \\ \dot{\phi}_2 \\ \dot{\phi}_3 \end{bmatrix} = \frac{1}{r_w} \begin{bmatrix} \sin(\theta) & -\cos(\theta) & -R \\ \sin(\theta + \frac{2\pi}{3}) & -\cos(\theta + \frac{2\pi}{3}) & -R \\ \sin(\theta + \frac{4\pi}{3}) & -\cos(\theta + \frac{4\pi}{3}) & -R \end{bmatrix} \begin{bmatrix} \dot{x} \\ \dot{y} \\ \dot{\theta} \end{bmatrix} \quad (3.8)$$

## 3.2 Dynamics

Now we map joint forces to Cartesian forces. The base's free-body diagram is shown in Figure 3.2. It is similar to Figure 3.1, but we have replaced velocities with forces;  $F_i$  represents the reaction force of wheel  $i$ .

From the diagram, we can state the following:

$$F_x = M\ddot{x} = \sum_{i=1}^3 F_{i,x} \quad (3.9)$$

$$F_y = M\ddot{y} = \sum_{i=1}^3 F_{i,y} \quad (3.10)$$

$$M_z = J_z\ddot{\theta} = -\sum_{i=1}^3 F_i R \quad (3.11)$$

where  $M$  is the mass of the base and  $J_z$  is its moment of inertia around the  $z$ -axis.

We can obtain  $F_{i,x}$  and  $F_{i,y}$  below:

$$F_{i,x} = F_i \sin(\theta + \alpha_i) \quad (3.12)$$

$$F_{i,y} = -F_i \cos(\theta + \alpha_i) \quad (3.13)$$

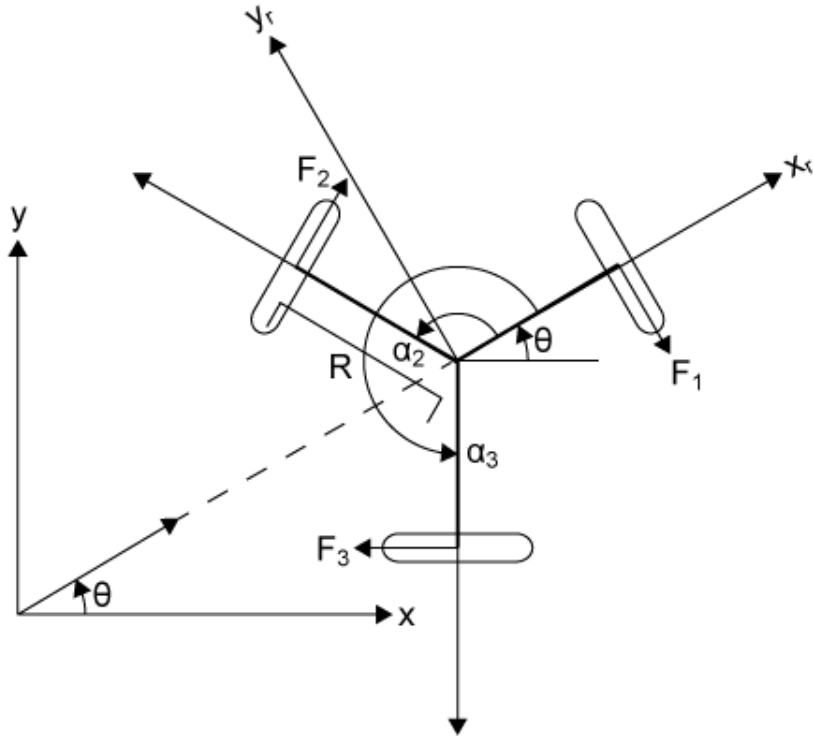


Figure 3.2: Trikey dynamics

Representing actuated wheel torque, or joint torque, as  $\tau_i$ , we get the following:

$$F_i = \frac{\tau_i}{r_w} \quad (3.14)$$

Now we plug 3.12, 3.13, and 3.14 into 3.9, 3.10, and 3.11. Substituting values for  $\alpha_i$  and simplifying and rearranging to matrix form, we get the following:

$$\begin{bmatrix} F_x \\ F_y \\ M_z \end{bmatrix} = \begin{bmatrix} M & 0 & 0 \\ 0 & M & 0 \\ 0 & 0 & J_z \end{bmatrix} \begin{bmatrix} \ddot{x} \\ \ddot{y} \\ \ddot{\theta} \end{bmatrix} = \frac{1}{r_w} \begin{bmatrix} \sin(\theta) & \sin(\theta + \frac{2\pi}{3}) & \sin(\theta + \frac{4\pi}{3}) \\ -\cos(\theta) & -\cos(\theta + \frac{2\pi}{3}) & -\cos(\theta + \frac{4\pi}{3}) \\ -R & -R & -R \end{bmatrix} \begin{bmatrix} \tau_1 \\ \tau_2 \\ \tau_3 \end{bmatrix} \quad (3.15)$$

Rearranging in terms of joint torques, we get the following:

$$\begin{bmatrix} \tau_1 \\ \tau_2 \\ \tau_3 \end{bmatrix} = r_w \begin{bmatrix} \sin(\theta) & \sin(\theta + \frac{2\pi}{3}) & \sin(\theta + \frac{4\pi}{3}) \\ -\cos(\theta) & -\cos(\theta + \frac{2\pi}{3}) & -\cos(\theta + \frac{4\pi}{3}) \\ -R & -R & -R \end{bmatrix}^{-1} \begin{bmatrix} M & 0 & 0 \\ 0 & M & 0 \\ 0 & 0 & J_z \end{bmatrix} \begin{bmatrix} \ddot{x} \\ \ddot{y} \\ \ddot{\theta} \end{bmatrix} \quad (3.16)$$

$$\begin{bmatrix} \tau_1 \\ \tau_2 \\ \tau_3 \end{bmatrix} = r_w \begin{bmatrix} \sin(\theta) & \sin(\theta + \frac{2\pi}{3}) & \sin(\theta + \frac{4\pi}{3}) \\ -\cos(\theta) & -\cos(\theta + \frac{2\pi}{3}) & -\cos(\theta + \frac{4\pi}{3}) \\ -R & -R & -R \end{bmatrix}^{-1} \begin{bmatrix} F_x \\ F_y \\ M_z \end{bmatrix} \quad (3.17)$$

Now, using Equations 3.16 and 3.17, we can specify global control actions in terms of forces or accelerations and know what torques we should apply at the joint level (wheels).

One should note that the relationship,

$$\begin{bmatrix} F_x \\ F_y \\ M_z \end{bmatrix} = \begin{bmatrix} M & 0 & 0 \\ 0 & M & 0 \\ 0 & 0 & J_z \end{bmatrix} \begin{bmatrix} \ddot{x} \\ \ddot{y} \\ \ddot{\theta} \end{bmatrix} \quad (3.18)$$

assumes that the system is unconstrained; in other words, inertias of the wheels and powertrain components are neglected. In reality, if forces and accelerations are applied to the base in Cartesian coordinates, wheels and powertrain components are forced to turn as well, increasing the effective inertia beyond simply  $M$  or  $J_z$ .

# Chapter 4

## Control

Now that Trikey has been built, it must be controlled. This chapter describes the control architecture, in terms of both hardware and software, that is used to control Trikey.

Trikey's overall control architecture has gone through two major revisions. The first utilized HCRL-MC motor control boards for low-level control of each wheel, in addition to a computer with Ubuntu-RTAI that handled higher level control and commanded each HCRL-MC via serial communication. Custom high-level control programs were written to run in RTAI. Basic current control of the motors was achieved using this architecture.

The second (and current) revision utilizes control boards and M3 control software developed by Meka Robotics. The M3 software has been integrated with whole-body control software jointly developed between Stanford and UT Austin [30] to implement whole-body control algorithms [32] on the base. The same framework can also control the base together with the Dreamer upper-body.

### 4.1 Version 1: HCRL-MC/Ubuntu RTAI

In this section we describe the control architecture utilizing the HCRL-MC motor control boards and custom high-level control programs written for Ubuntu-RTAI.

#### 4.1.1 Hardware

The HCRL-MC is a custom motor control board designed by Nicholas Paine, of the Human-Centered Robotics Lab, for position, velocity, current, and torque control of BLDC motors. The physical board layout and block diagram of its architecture are displayed in Figure 4.1. The architecture centers around a Freescale MC9S08MP16 microcontroller, which contains an 8-bit processor (HCS08 core), 16 kB flash memory, 1 kB RAM, and a 13 channel 12-bit ADC. Clock speed and PWM frequency are 50 MHz.

Current and torque control on the HCRL-MC are performed using a basic incremental control law, which increments the PWM duty cycle of the applied motor voltage if sensor input is less than the reference, and decrements the duty cycle if it is greater than the reference, with bounds at 0 (zero voltage) and 255 (full voltage).

Communication between the HCRL-MC and host computer takes place using a custom RS-232 serial communication protocol, with the HCRL-MC acting as a slave device to the host master. For the three HCRL-MCs that are needed for Trikey, each one can connect separately to the host via separate serial ports (if available on the host computer). Alternatively, two or more boards can be daisy-chained together via the I2C bus available on each board. In this case, one board acts as a proxy that sends and receives messages on behalf of the other boards, which are identified in the communication protocol via their board ID number. This communication topology is displayed graphically in Figure 4.2.

#### 4.1.2 Software

Though each HCRL-MC can handle low-level control of a single wheel, a computer is needed to implement higher-level control programs that decide the joint-level

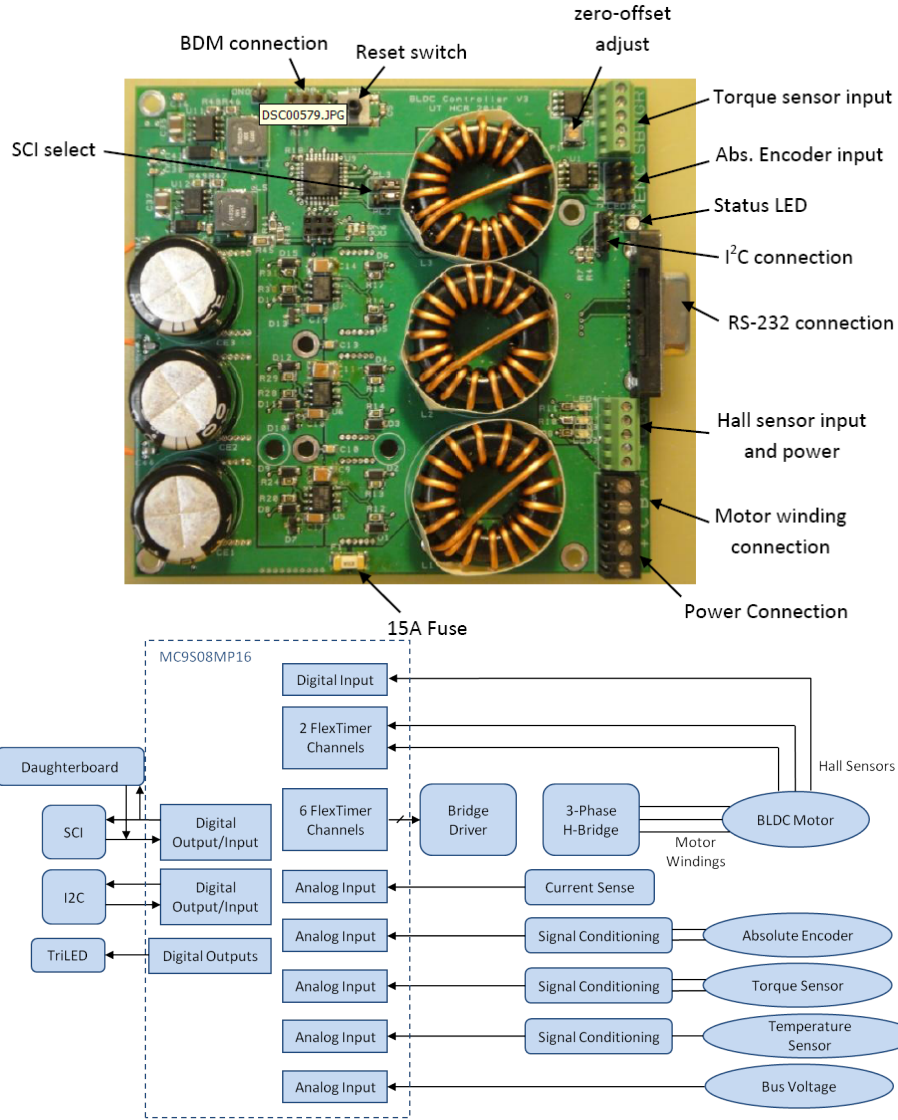


Figure 4.1: HCRL-MC **Above:** Physical board layout and connections. **Below:** Block diagram specification of board. A computer sends the processor (MC9S08MP16) target torque/velocity signals over the serial communication interface (SCI). Additional motor controllers communicate with the processor via inter-integrated circuit bus (I<sup>2</sup>C). Various sensors can send data such as torque and circuit temperature to the processor. The processor sends a pulse-width modulated voltage control signal to the brushless DC (BLDC) motor in response to these inputs. The motor is commutated and driven using the hall sensor input signals (to determine rotor position) and H-bridge circuit.

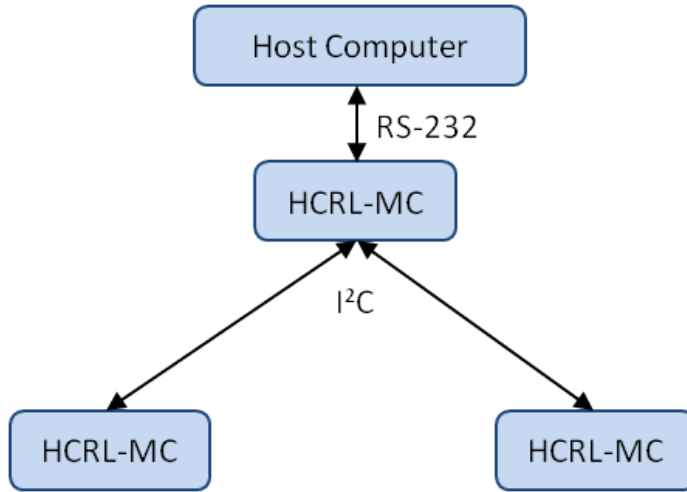


Figure 4.2: Daisy-chaining multiple HCRL-MCs

commands for wheel. For such programs to be functional, they need to operate within a system that can guarantee timing constraints. One option that can be used to achieve this is to use a real-time operating system (RTOS) such as VxWorks, Enea OSE, Lynx OS, or QNX. For Trikey, it was decided to adopt RTAI (Real Time Application Interface for Linux), which though not strictly an RTOS, is a community-developed open-source interface that patches a standard Linux kernel and allows users to write applications with strict timing constraints. Real-time code is usually run using dynamically loadable kernel modules.

RTAI was installed in Ubuntu 10.04, running on an Advanced Digital Logic ADL945HD 3.5" form factor single-board, industrial computer. To develop and test applications to control the base, a kernel module was developed that handles communication with the HCRL-MC. Once loaded, the kernel module acts as a "serial server" for a particular serial port and handles all communication for that port. The module allocates two shared memory structures - one for reading, one for writing - that allow user programs to read from and write data to an HCRL-MC connected

to the serial port. To use multiple ports, multiple instances of the kernel module must be loaded. At a predefined, constant frequency, any new data placed in the write structure by a user application is sent to the HCRL-MC, and any responses received from the HCRL-MC are parsed and placed in the read structure. More than one HCRL-MC can be communicated with via a single serial port if the I2C bus is used, at the expense of serial bandwidth. In this case, an array of shared memory structures are used to distinguish data sent to and received from different boards.

The use of the kernel module to handle communication follows the “separation of concerns” software design philosophy by separating communication from computation; once the appropriate kernel modules are loaded, user-written control code can simply read and write to shared memory without dealing with the specifics of HCRL-MC communication. This is shown in Figure 4.3, which demonstrates how a user program can control the motors in a configuration utilizing two serial ports (COM1 and COM2) of the computer.

To test basic compliant control of the base, a control program was written that sends sinusoidal reference currents to each wheel. By doing this, the base can move smoothly back and forth from a home position, but react safely and compliantly if an obstacle interrupts its trajectory. Figure 4.4 shows the tracking success of a single wheel of the base when moving on the floor.

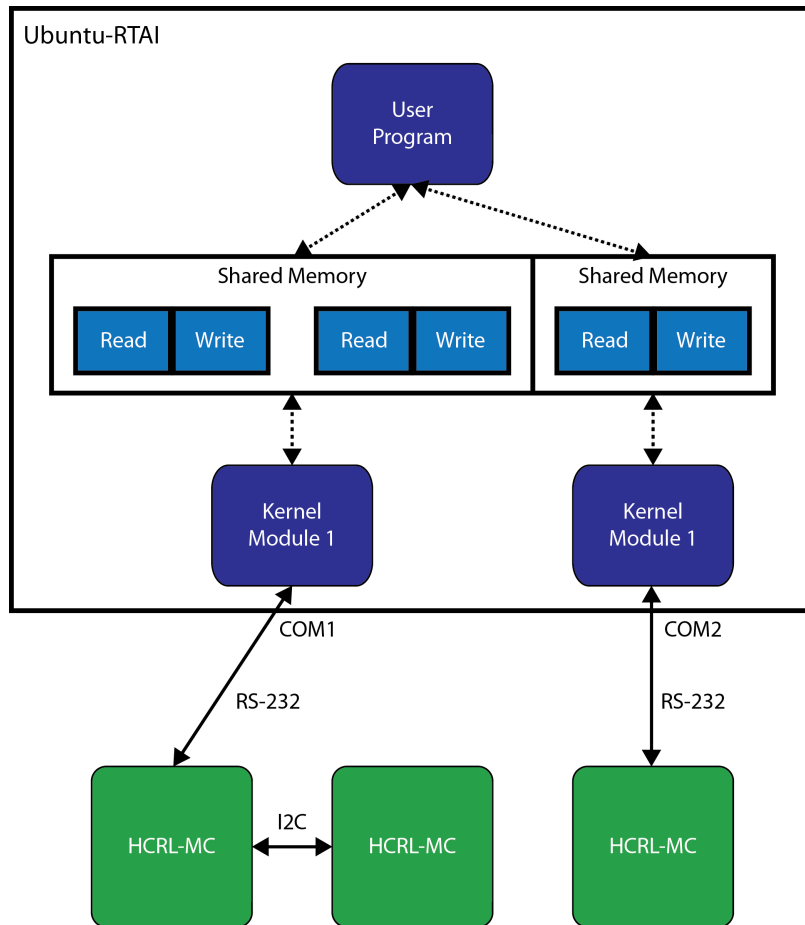


Figure 4.3: Architecture of custom control software in RTAI

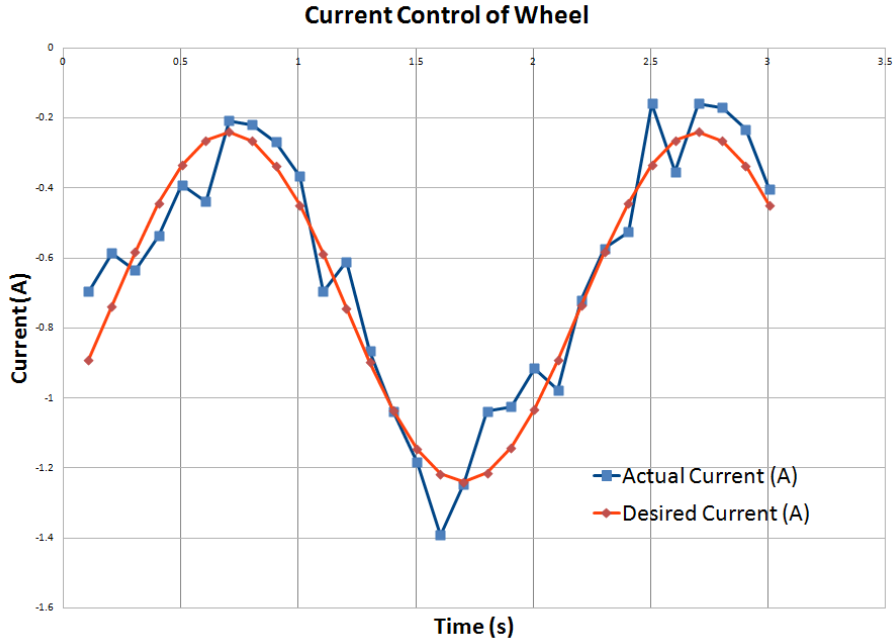


Figure 4.4: Current control of single wheel. Data is sampled at 10 Hz.

## 4.2 Version 2: M3/WBC control

In order to facilitate ease of long-term maintenance, the control architecture utilizing the HCRL-MC and Ubuntu with RTAI was replaced with a power system, control electronics and M3 control software supplied by Meka Robotics, used in conjunction with custom open-source whole-body control software. In this section we briefly describe the hardware and software supplied by Meka, as well as its integration with custom control software.

### 4.2.1 Hardware

The hardware supplied by Meka includes the following components:

- An AC-DC power supply for powering the base and upper body together, and/or charging lead acid batteries placed inside

- A DC-DC power board for distributing power between the base and upper body, seamlessly switching between wall and battery power, and connecting emergency stops
- A smaller power board for just the base, which powers the motor controllers, integrates sensor signals, and handles EtherCAT communication between the base and real-time PC (or an EtherCAT hub as an intermediary)
- A Beckhoff EtherCAT hub that can plug into both the base and upper body, and connect a single EtherCAT cable from a real-time PC to the entire base/upper body system
- An amplifier board for the three load cells, which plugs into the smaller power board
- Three motor controllers, which replace the HCRL-MC for driving the three motors
- Two emergency stops - one to be placed on the base itself, and another remote emergency stop to be used by the robot operator. Pressing or unplugging either emergency stop cuts power to the motors.
- One 3DM-GX3-25 high-performance miniature Attitude Heading Reference System (AHRS), made by MicroStrain. The AHRS includes a 3-axis accelerometer, 3-axis gyroscope, 3-axis magnetometer, and temperature sensors (for temperature compensation). An on-board processor utilizes sensor fusion algorithms to provide fully calibrated static and dynamic orientation and inertial measurements, which aids trajectory tracking with respect to a global coordinate frame.

In place of the RS-232 serial communication protocol used by the HCRL-MC for real-time PC communication, the Meka hardware utilizes EtherCAT (Ethernet for Control Automation Technology). EtherCAT is a high-speed fieldbus system that works on existing Ethernet physical infrastructure. More information about EtherCAT technology is available in [19].

#### 4.2.2 Software

Meka’s hardware is paired with its M3 control software. M3, which also happens to run in Ubuntu-RTAI, effectively replaces the custom kernel module described in section 4.1. M3 utilizes a shared memory interface to receive joint torque commands from user programs, and also to send back joint data (motor currents, load cell values, encoder values) and AHRS data (the orientation matrix and accelerometer, gyroscope, and magnetometer data).

In our case, the user program is an extension of the whole-body control software package described in [30]. The interface between the whole-body control software and M3 is the RTUtil process, which runs a real-time loop in RTAI and reads and writes to M3’s shared memory interface. Communication between RTUtil and the whole-body controller is handled by the Servo process, which instantiates a Servo object as well as Model, Controller, Skill, and Task objects. Each Task is an operational-space controller that drives the robot toward some state, while a Skill determines the current task hierarchy. The Model contains estimates of the robot’s dynamics and kinematics (explored in Chapter 3) and aids the Controller in sending joint torques through Servo and RTUtil.

Before implementing full whole-body control, we were able to test the control architecture by removing the Model, Skills, and Tasks and setting up a simple PD joint-space controller that compliantly holds Trikey in position. The form of this

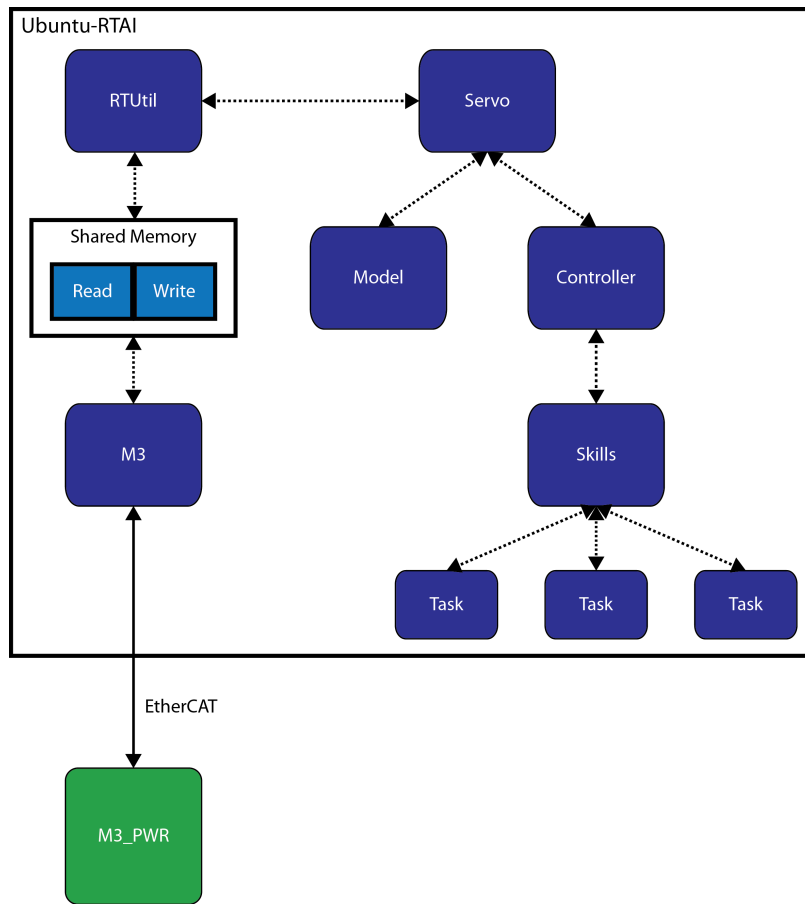


Figure 4.5: Whole-body control architecture

controller is given by,

$$\boldsymbol{\tau}_{des} = K_p(\boldsymbol{\theta}_{des} - \boldsymbol{\theta}_{actual}) + K_d(\dot{\boldsymbol{\theta}}_{des} - \dot{\boldsymbol{\theta}}_{actual}) \quad (4.1)$$

where  $\boldsymbol{\tau}_{des}$  is the vector of desired torques at each wheel,  $\boldsymbol{\theta}_{des}$  is the vector of desired angular positions of each wheel, and  $\boldsymbol{\theta}_{actual}$  is the vector of measured angular positions of each wheel. Each wheel, then, acts as a linear rotational spring.

# Chapter 5

## Conclusions & Future Work

### 5.1 Summary of thesis

The preceding chapters presented the design and development of a holonomic mobile base, Trikey, that can interact compliantly with its environment, as well as support a force-controlled humanoid upper body that can do the same. A literature review, followed by a description of Trikey’s design evolution, revealed that Trikey is unique among existing mobile bases for possessing all of the following characteristics:

1. Fully holonomic (on a sufficiently flat and smooth surface that allows the wheels to remain in contact and the passive rollers to move)
2. Can directly sense external forces and torques using torque sensors at the wheels, rather than measuring motor current
3. Has the power and control infrastructure required to be controlled concurrently with a force-controlled humanoid upper body mounted on top
4. Minimalist but effective design employing relatively few parts

Design calculations concerning Trikey’s torque, velocity, power, and torque sensing requirements were described, and the selection of its wheels, motors, gearboxes, torque sensors, torque limiters, and couplings was presented. We derived Trikey’s kinematic and dynamic models, which were used to make design decisions for the base and implemented in its controllers. We also described two versions of Trikey’s control

architecture, the first of which utilized custom hardware and software, while the second utilizes hardware and control software supplied by a vendor but interfaces with custom high-level control software. Simple experiments demonstrated that safe, compliant control is possible with both versions.

## 5.2 Future work

### 5.2.1 Control

With Dreamer mounted on Trikey, the two together compose a mobile humanoid manipulation platform where, due to direct torque or force sensing at nearly every joint (with the exception of the position-controlled humanoid head), the internal and external dynamics of the system can be known with a high degree of accuracy. This opens up possibilities for implementing mobile whole-body compliant skills that control the system’s center of mass, execute operational space tasks in a prioritized fashion at multiple contact points, and control internal forces [33].

As noted in 3.2, the dynamic model derived in that section assumes an unconstrained system. For better system performance, the constrained system dynamics would need to be derived, augmenting the inertia matrix in Equation 3.18 to account for the rotational inertias of the wheels and powertrain components. Furthermore, modeling the base as a free-floating virtual linkage [43] in 3D space and utilizing data from the AHRS would allow for operational space control in three dimensions, even though the base can only be actuated at a planar level. This would allow Trikey and Dreamer to react to gentle slopes and even loss of contact of a wheel. For example, Dreamer could erase a whiteboard with smooth motions of its hand and arm, even if during this task, Trikey must maneuver on an irregular or gently sloping floor in front of the whiteboard. As described in 4.2, the basic software and hardware infrastructure already exists to implement the extended models and advanced controllers

needed to perform such tasks.

### 5.2.2 Design

Though Trikey's design is functional, there are several improvements that could be made to increase its robustness and capabilities. Replacing the exposed miter gears with enclosed gearboxes would increase robustness and decrease backlash and frictional losses. Custom omni wheels with larger rollers would let Trikey traverse rougher terrain, and vibrations could be substantially reduced by adopting Song and Byun's continuous alternate wheel (CAW) design [3]. Implementing custom compliant torque sensors, as discussed in 2.4.3, would eliminate the bulky torque limiters and load cells and increase Trikey's shock tolerance. Adding a vertical linear spring (i.e. suspension), along with a sensor to measure its displacement, to each power/sensing module would allow for the accurate detection of loss of contact of a wheel, in addition to better vertical shock tolerance and terrain traversal.

## Appendices

# Appendix A

## Operating Instructions

As of December 2011, here are the instructions to operate Trikey with its whole-body control software. A PC running Ubuntu with RTAI, Meka’s M3 control software, and ROS is required. ROS (Robot Operating System) is used by the whole-body control software.

M3 utilizes the EtherLab EtherCAT master to get data from the EtherCAT bus connecting the controller boards. The PC should have a Realtek Ethernet chipset in order to work with the EtherLab master.

The instructions assume that the user has already checked Trikey’s internal wiring and turned on and logged into Ubuntu on the PC.

1. Make sure at least one of the E-stops is activated (pushed down). Set the red DPST switch to the ”ON” position, if it isn’t already.
2. Check the EtherCAT connection between Trikey and the PC, and turn on the digital power switch. The LEDs on the digital power board should light up. If the connection is working, within a few seconds the LEDs should start flashing rapidly.
3. Open a terminal window in Ubuntu, and enter

```
m3rt_server_run -m
```

This starts the M3 real-time server. The `-m` command places all components in shared memory in operational mode.

4. In another terminal window, enter

```
roscore
```

This starts the ROS Master.

5. In another terminal window, `cd` to to whatever directory contains the

`whole_body_control` folder. To run a skill on Trikey, enter

```
cd whole_body_control/wbc_m3_ctrl
```

```
./bin/servo_base -v -r base_config/trikey.xml -s base_config/  
skill.yaml
```

where *skill.yaml* is the skill file you want to run. The **-v** option indicates verbose mode, **-r** indicates robot specification (which is contained in **trikey.xml**), and **-s** indicates skill specification.

6. Release the activated E-stop and watch Trikey perform the skill. Be prepared to hit the E-stop if something goes wrong.
7. Hit the E-stop when you're done with the skill. Run another skill, or **Ctrl-C** out of the three terminal windows if you're done.

## Appendix B

### Wiring Information

This appendix describes how to put together Trikey's control electronics (supplied by Meka), and connect them to the motors, torque sensors, encoders, and AHRS.

Ref.	Description	Mfr. Part Number	Usage	Manufacturer
1	3 position, white	54483-3	Motor windings	TE Connectivity
2	1 position, black	53894-2	Motor wire shield	TE Connectivity
3	12 AWG solder crimp	54329-1	Connect wires to (1) and (2)	TE Connectivity
4	5 position JST	GHR-05V-S	Hall sensors/encoders/torque sensors/AHRS	JST
5	26-30 AWG crimp	SSHL-002T-P0.2	Connect wires to (4)	JST
6	5x2 pin, black	FFSD-05-D-36.00-01-N	AHRS	Samtec
7	5-pin finger latching	CON-FC5-28	Encoder	US Digital
8	Metal circular w/ cable clamp	PT06A-12-10S(SR)	Torque sensors	Amphenol Industrial

Table B.1: Connectors for electronics

Ref.	Description	Mfr. Part Number	Usage	Supplier
9	Hand crimp for (4)	YRS-1140	JST Crimp, 26-30 AWG	JST
10	Hand crimp for (4)	TOL-10219	General crimp for very small 1.25-2.5mm crimp pins	SparkFun Electronics

Table B.2: Recommended crimp tools

# Mobile Base **mekā** Wiring Assembly

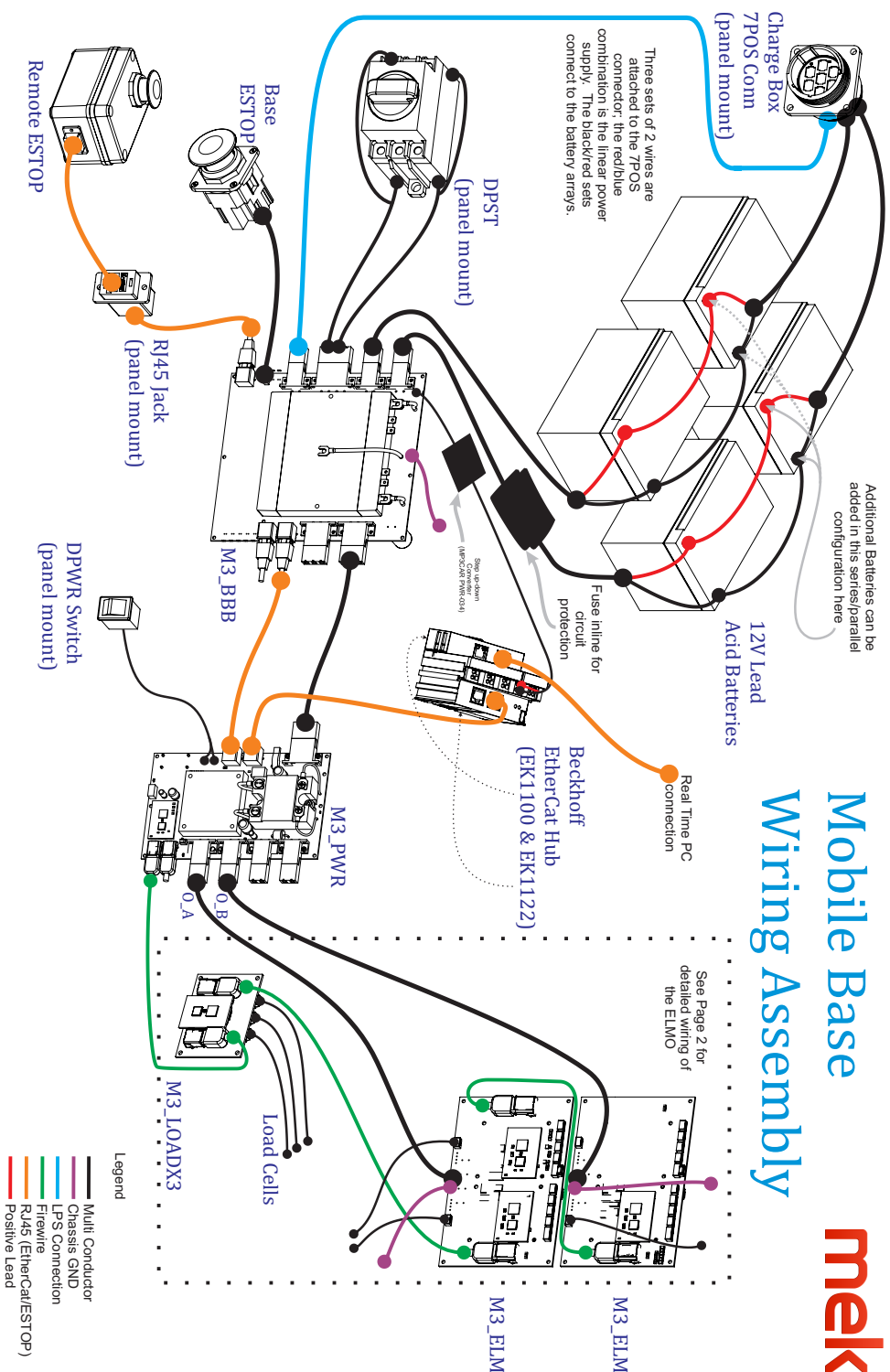
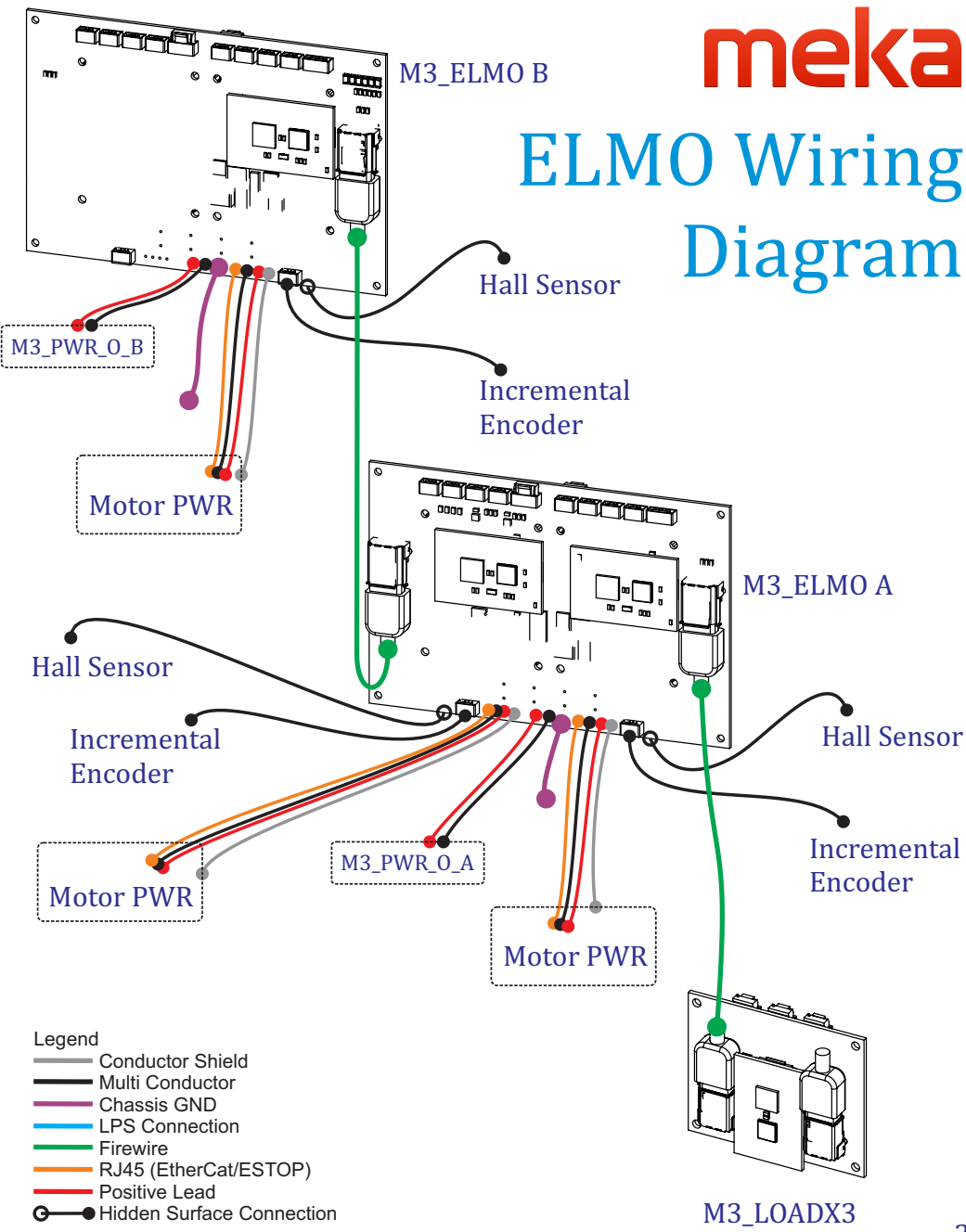


Figure B.1: System wiring overview

**meka**

## ELMO Wiring Diagram



2

Figure B.2: ELMO motor controller wiring. J0, J1, and J2 (as marked on the M3\_ELMO boards) should connect to Motors 1, 2, and 3 (as marked on the motors), respectively, as well as their respective hall sensors and encoders. The torque sensor of the motor connected to J0 should connect to LOAD\_A on the M3\_LOADX3 board; similarly, J1 corresponds to LOAD\_B and J2 corresponds to LOAD\_C.

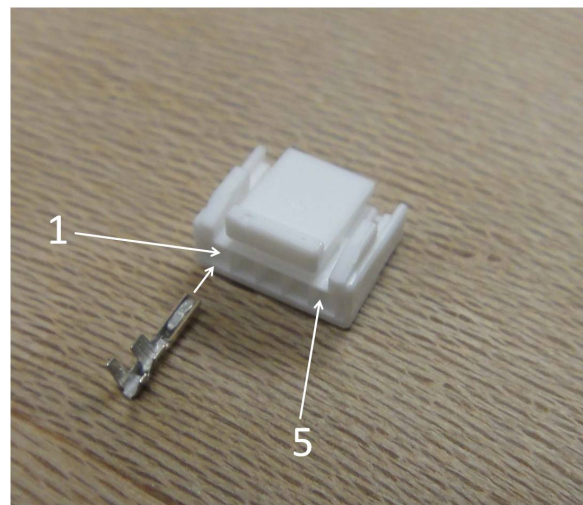


Figure B.3: Pin order and connection information for 5-position JST connector. The white JST connector shown ((4) in Table B.1) is used by the motor hall sensors, torque sensors, encoders, and AHRS to connect to the Meka control boards. Multiconductor 26-30 AWG cabling links the JST connector to the appropriate connector of each sensor. Each individual wire should be crimped to the JST crimp shown ((5) in Table B.1), which is then inserted into the appropriate pin position on the connector. The recommended crimping tools for accomplishing this are (9) or (10) in Table B.2. The pin order defined in this figure is assumed by the pinout tables that follow in this appendix.

## B.1 Motor Wiring

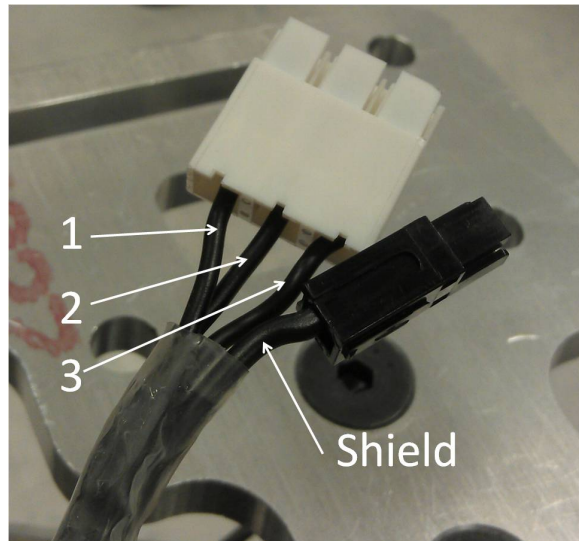


Figure B.4: Motor winding wiring. The wires from the three windings of the Maxon BLDC motor are numbered, and they connect to the white 3-position connector ((1) in Table B.1) as shown. Each wire is soldered onto a solder crimp ((3) in Table B.1), which then snaps into place inside (1). A separate 12 AWG wire is soldered onto the shielding of the motor winding multiconductor cable and attaches to the black connector shown ((2) in Table B.1). (1) and (2) connect to the "Multi Conductor" and "Conductor Shield" wires coming from the ELMO motor controllers, as shown in Figure B.2.

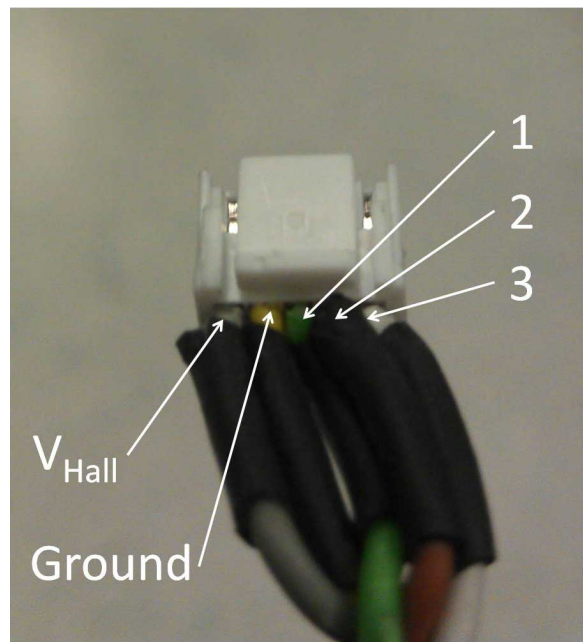


Figure B.5: Hall sensor wiring. The wires from the hall sensor on the Maxon BLDC motor connect to the JST connector ((4) in Table B.1) as shown. The JST connector plugs into one of the M3\_ELMO boards; see Figure B.2. Wire colors, from left to right, are the following: gray, yellow, green, brown, white. For more information on how to attach the wires to the connector, see Figure B.3.

## B.2 Torque Sensor Wiring

Pin	Function
1	– Signal
2	+ Signal
3	Ground/Shield
4	Ground/Shield
5	+ Excitation

Table B.3: Pinout for JST connector for torque sensor. Connector is (4) in Table B.1. The JST connector plugs into the M3\_LOADX3 board; see Figure B.2. Note that pins 3 and 4 are connected together on the M3\_LOADX3 board. Pin order and connection information are given in Figure B.3.

Pin	Function
A	+ Excitation
B	– Excitation
C	+ Signal
D	– Signal

Table B.4: Pinout for circular connector for torque sensor. Connector is (8) in Table B.1. Plugs into torque sensor. Note that there is no – Excitation on the M3\_LOADX3, so pin B can connect to Ground. The pin letters are marked on the connector itself and wiring is self-evident.

### B.3 Encoder Wiring

Pin	Function
1	B channel
2	+5VDC
3	A channel
4	Index
5	Ground

Table B.5: Pinout for JST connector for encoder. Connector is (4) in Table B.1. Plugs into one of the M3\_ELMO boards; see Figure B.2. Pin order and connection information are given in Figure B.3.

Pin	Function
1	Ground
2	Index
3	A channel
4	+5VDC
5	B channel

Table B.6: Pinout for CON-FC5 connector for encoder. Connector is (7) in Table B.1. Plugs into encoder. Pin order and connection information are given in Figure B.6.

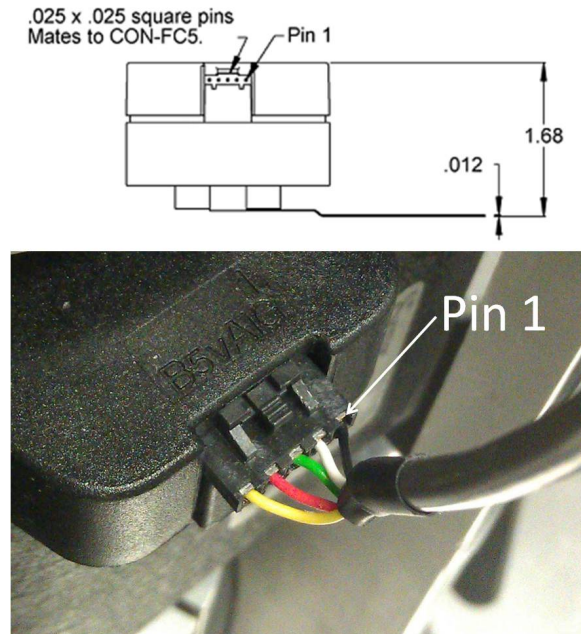


Figure B.6: Pin order and connection information for CON-FC5 connector. Connector ((7) in Table B.1) comes with a "finger" for each pin. Each wire can be pressed/soldered into the appropriate finger, which is then inserted and locks into place inside the connector. Connector is inserted into the encoder in the orientation shown by pressing down the ridged tab and is removed easily the same way. The last part of the connector part number (i.e. after FC5) specifies the AWG of the wires that should be used (though, in practice, a range is possible). Dimensions shown are in inches.

## B.4 AHRS Wiring

Pin	Function
1	Ground
2	AHRS_UART_RX
3	AHRS_UART_TX
5	+3.3VDC

Table B.7: Pinout for JST connector for AHRS. Connector is (4) in Table B.1. Plugs into the M3\_PWR board, though this is not shown in Figure B.1. Pin order and connection information are given in Figure B.3.

Pin	Function
3	+3.3VDC
4	AHRS_UART_RX
5	AHRS_UART_TX
8	Ground

Table B.8: Pinout for 5x2 pin connector for AHRS. Connector is (6) in Table B.1. Plugs into AHRS. Pin order and connection information are given in Figure B.7.

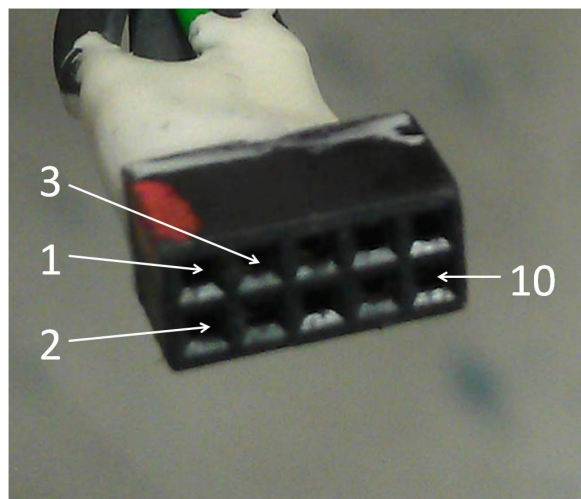


Figure B.7: Pin order and connection information for AHRS 5x2 pin connector. Connector is (6) in Table B.1. Plugs into AHRS by aligning the red dot (indicating pin 1) with the white dot on the AHRS. Note that the part number in Table B.1 actually specifies a ribbon cable with this connector on its end.

## Appendix C

### Component Specifications

Part	Mfr. Part Number	Manufacturer
BLDC Motor	136207	Maxon
43:1 Planetary gearbox	203120	Maxon
Coupling	BKL30	R+W
2500 ppr Encoder	E6-2500-1000-I-S-H-T-B	US Digital
Torque sensor	01324-052	Sensor Developments
Torque limiter	SK2	R+W
Miter gear	6529K22	McMaster-Carr
Omni wheel	am-0559	AndyMark
AHRS	3DM-GX3-25	MicroStrain

Table C.1: Major component list

## EC 45 Ø45 mm, brushless, 250 Watt, CE approved

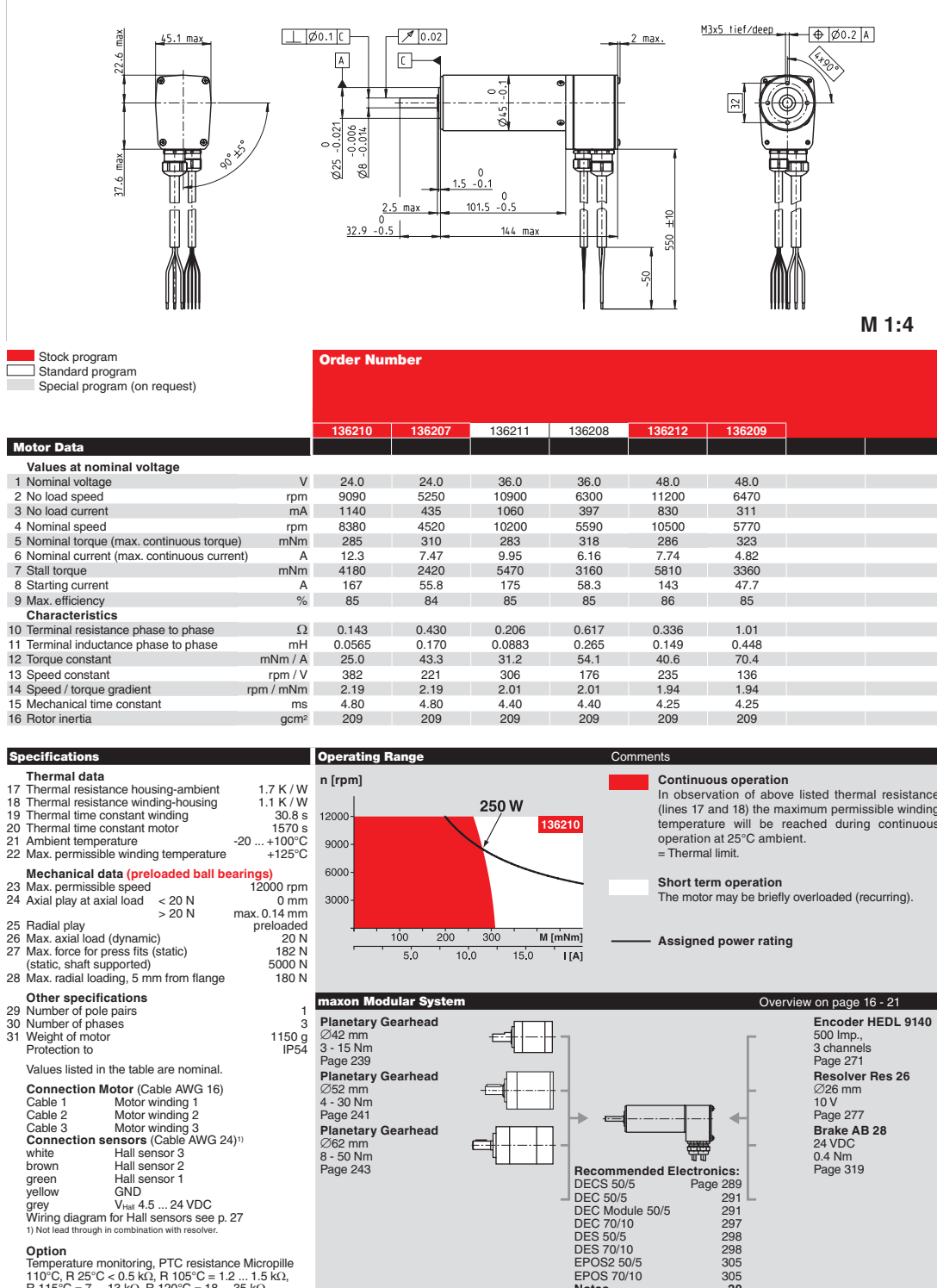
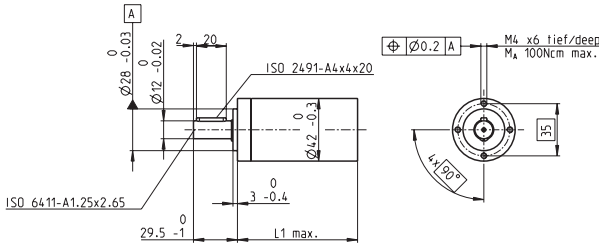


Figure C.1: Snapshot of motor mfr. datasheet. Part number is 136207.

## Planetary Gearhead GP 42 C Ø42 mm, 3 - 15 Nm

Ceramic Version



### Technical Data

Planetary Gearhead	straight teeth
Output shaft	stainless steel
Bearing at output	preloaded ball bearings
Radial play, 12 mm from flange	max. 0.06 mm
Axial play at axial load	< 5 N 0 mm > 5 N max. 0.3 mm
Max. permissible axial load	150 N
Max. permissible force for press fits	300 N
Sense of rotation, drive to output	=
Recommended input speed	< 8000 rpm
Recommended temperature range	-40 ... +100°C
Number of stages	1 2 3 4
Max. radial load, 12 mm from flange	120 N 150 N 150 N 150 N

M 1:4

- Stock program
- Standard program
- Special program (on request)

### Gearhead Data

1 Reduction	3.5 : 1	12 : 1	26 : 1	43 : 1	81 : 1	156 : 1	150 : 1	285 : 1	441 : 1	756 : 1
2 Reduction absolute	7/2	49/4	26	343/8	2197/27	156	2401/16	15379/54	441	756
10 Mass inertia	gcm <sup>2</sup>	14	15	9.1	15	9.4	9.1	15	15	14
3 Max. motor shaft diameter	mm	10	10	8	10	8	8	10	10	10

### Order Number

	203113	203115	203119	203120	203124	203129	203128	203133	203137	203141

### Order Number

	203114	203116	260552*	203121	203125	260553*	203130	203134	203138	203142

### Order Number

	260551*	203117	203122	203126	203131	203135	203139	260554*

### Order Number

	1	2	3	3	3	4	4	4	4

### Order Number

	203118	203123	203127	203132	203136	203140

### Order Number

1 Reduction	21 : 1	74 : 1	126 : 1	257 : 1	394 : 1	676 : 1
2 Reduction absolute	21	147/2	126	1029/4	1183/3	676

### Order Number

10 Mass inertia	gcm <sup>2</sup>	4.9	9.4	15	5.0	15	9.4	14	5.0
3 Max. motor shaft diameter	mm	4	8	10	8	10	8	10	4

### Order Number

1 Reduction	1	2	2	3	3	3	4	4	4
2 Reduction absolute	21	147/2	126	1029/4	1183/3	676			

### Order Number

10 Mass inertia	gcm <sup>2</sup>	14	15	14	15	15	15	9.1	
3 Max. motor shaft diameter	mm	10	10	10	10	10	10	8	

### Order Number

4 Number of stages	1	2	2	3	3	3	4	4	4
5 Max. continuous torque	Nm	3.0	7.5	7.5	15.0	15.0	15.0	15.0	15.0

### Order Number

6 Intermittently permissible torque at gear output	Nrn	4.5	11.3	11.3	22.5	22.5	22.5	22.5	22.5
7 Max. efficiency	%	90	81	81	72	72	72	64	64

### Order Number

8 Weight	g	260	360	360	460	460	560	560	560
9 Average backlash no load	°	0.6	0.8	0.8	1.0	1.0	1.0	1.0	1.0

### Order Number

11 Gearhead length L1	mm	41.0	55.5	55.5	70.0	70.0	70.0	84.5	84.5
* no combination with EC 45 (150 W and 250 W)									



### maxon Modular System

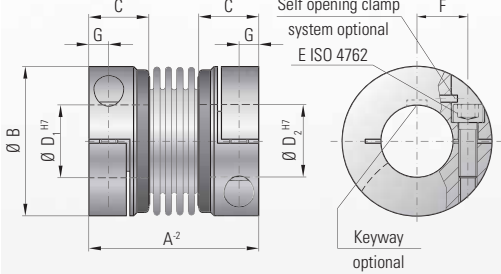
+ Motor	Page	+ Sensor	Page	+ Brake	Page	Overall length [mm]	= Motor length + gearhead length + (sensor / brake) + assembly parts
EC 45, 250 W	156					185.1	199.6
EC 45, 250 W	156	HEDL 9140	271			200.7	215.2
EC 45, 250 W	156	Res 26	277			185.1	199.6
EC 45, 250 W	156			AB 28	319	192.5	207.0
EC 45, 250 W	156			AB 28	319	209.5	224.0
EC-max 30, 60 W	167					105.1	119.6
EC-max 30, 60 W	167	MR	262			117.3	131.8
EC-max 30, 60 W	167	HEDL 5540	269			125.7	140.2
EC-max 30, 60 W	167			AB 20	316	141.3	155.8
EC-max 30, 60 W	167	HEDL 5540	269	AB 20	316	162.1	176.6
EC-max 30, 60 W	167					99.1	113.6
EC-max 40, 70 W	168					115.0	129.5
EC-max 40, 70 W	168	MR	263			122.5	137.0
EC-max 40, 70 W	168	HEDL 5540	269			137.0	151.5
EC-max 40, 70 W	168			AB 28	317	139.1	153.6
EC-max 40, 70 W	168	HEDL 5540	269	AB 28	317	162.5	177.0
EC-4pole 30, 100 W	175					88.1	102.6
EC-4pole 30, 100 W	175	MR	262			100.3	114.8
EC-4pole 30, 100 W	175	HEDL 5540	270			108.7	123.2
EC-4pole 30, 100 W	175			AB 20	316	124.3	138.8
EC-4pole 30, 100 W	175					145.1	159.6
EC-4pole 30, 200 W	176					105.1	119.6
EC-4pole 30, 200 W	176	MR	262			117.3	131.8
EC-4pole 30, 200 W	176	HEDL 5540	270			125.7	140.2
EC-4pole 30, 200 W	176			AB 20	316	141.3	155.8
EC-4pole 30, 200 W	176					161.1	175.6
MCD EPOS, 60 W	313					161.1	175.6
MCD EPOS P, 60 W	313					161.1	175.6

Figure C.2: Snapshot of gearbox mfr. datasheet. Part number is 203120.



## MODEL BKL

**BACKLASH-FREE, TORSIONALLY STIFF METAL BELLOWS COUPLINGS**



**Ordering example**

**BKL / 80 / 26 / 22 / XX**

Model  
Series/Nm  
Ø D1 H7  
Ø D2 H7  
non standard



with clamping hub

**Properties:**

- easy to mount
- low moment of inertia
- economically priced

**Material:**  
Bellows made of highly flexible high-grade stainless steel. Hub material see table

**Design:**  
With a single ISO 4762 radial clamping screw per hub.

**Self opening clamp system optional:**  
**Loosening the clamping screw applies force to the pin, which will force the clamp into the open position for easy mounting and dismounting.**

**Temperature range:**  
-30 to +100° C (-22 F to 212 F)

**Speeds:**  
Up to 10,000 rpm, in excess of 10,000 with a finely balanced version.

**Backlash:**  
Absolutely backlash-free due to frictional clamped connection.

**Brief overloads:**  
Acceptable up to 1.5 times the value specified.

**Service life:**  
These couplings have an infinite life and are maintenance-free if the technical ratings are not exceeded.

**Tolerance:**  
On the hub/shaft connection 0.01 to 0.05 mm.

**Non standard:**  
Custom designs with varied tolerances, keyways, non-standard material, bellows and ATEX designs are available upon request.

Model BKL	Series										
	2	4.5	10	15	30	60	80	150	300	500	
Rated torque (Nm)	T <sub>KN</sub>	2	4.5	10	18	30	60	80	150	300	500
Overall length (mm)	A	30	40	44	58	68	79	92	92	109	114
Outer diameter (mm)	B	25	32	40	49	56	66	82	82	110	123
Fit length (mm)	C	10.5	13	13	21.5	26	28	32.5	32.5	41	42.5
Inner diameter possible from Ø to Ø H7 (mm)	D <sub>1/2</sub>	4-12.7	6-16	6-24	8-28	10-32	14-35	16-42	19-42	24-60	35-62
Fastening screw ISO 4762	E	M3	M4	M4	M5	M6	M8	M10	M10	M12	M16
Tightening torque of the fastening screw (Nm)	F	2.3	4	4.5	8	15	40	70	85	120	200
Distance between centers (mm)	G	8	11	14	17	20	23	27	27	39	41
Distance (mm)	G	4	5	5	6.5	7.5	9.5	11	11	13	17
Moment of inertia (10 <sup>-3</sup> kgm <sup>2</sup> )	J <sub>total</sub>	0.002	0.007	0.016	0.065	0.12	0.3	0.75	1.8   0.8	7.5   3.1	11.7   4.9
Hub material		AL optional steel	steel optional AL	steel optional AL	steel optional AL	steel optional AL					
Approx. weight (kg)		0.02	0.05	0.06	0.16	0.25	0.4	0.7	1.7   0.75	3.8   1.6	4.9   2.1
Torsional stiffness (10 <sup>3</sup> Nm/rad)	C <sub>t</sub>	1.5	7	9	23	31	72	80	141	157	290
axial ± (mm)		0.5	1	1	1	1	1.5	2	2	2	2.5
lateral ± (mm)	Max. values	0.2	0.2	0.2	0.2	0.2	0.2	0.2	0.2	0.2	0.2
angular ± (degree)		1	1	1	1	1	1	1	1	1	1
axial spring stiffness (N/mm)	C <sub>a</sub>	8	35	30	30	50	67	44	77	112	72
lateral spring stiffness (N/mm)	C <sub>l</sub>	50	350	320	315	366	679	590	960	2940	1450

(1Nm ≈ 8.85 in lbs)

Figure C.3: Snapshot of coupling mfr. datasheet. Part number is BKL30.

# 01324 Series

## ROTARY SHAFT TORQUE SENSOR

These sensors are designed to measure rotating drive torque using a conventional shaft-to-shaft configuration for in-line placement. The design incorporates a coin silver slip ring assembly that transmits excitation voltage to, and output signals from, the rotating sensor. These sensors can be supplied with Auto-ID, which eliminates scaling when used with the PTI or PMAC 2000 instruments. An optical encoder to measure angle or speed is also available with this model.

### SPECIFICATIONS

Capacity ..... 50 in. oz. to 20,000 in.lb. (See chart)  
 Overload capacity ..... 150% of F.S.  
 Output at F.S. ..... 2.0 mV/V nominal  
 Non-linearity ..... 0.10% of F.S.  
 Hysteresis ..... 0.10% of F.S.  
 Zero balance ..... 1.00% of F.S.  
 Compensated temperature ..... 70 to 170°F  
 Useable temperature ..... -65 to +250°F  
 Temperature effect on zero ..... 0.002% of F.S./°F  
 Temperature effect on span ..... 0.002% of Rdg./°F  
 Bridge resistance ..... 1000 Ohms  
 Excitation voltage, maximum ..... 20 Vdc  
 Maximum shaft speed ..... 5000 RPM\*

\*For faster shaft speeds and different end configurations, please contact the factory.

Mating connector supplied.



### OPTIONS

- 4 pin Bendix connector (non Auto-ID)
- 10 pin Bendix connector (Auto-ID)
- Integrated signal amplifier (+/-5V or +/-10V)
- Integral optical encoder - 1024 ppr and 1500 ppr (requires 10 pin connector)
- Footmount

### DIMENSIONS

MODEL	CAPACITY			SHAFT	KEY	MATERIAL
	IN-OZ.	IN-LBS	N-M			
01324-030	50	3	0.35	3/8"	1/32" flat	Stainless steel shafts/ Aluminum sensors
01324-060	100	6	0.71			
01324-120	200	12	1.41			
01324-310	500	30	3.53			
01324-620	1000	62	7.06			
01324-012	100	12	0.749	3/16"	1/4"	Steel
01324-022	200	23	0.999			
01324-052	500	56	1.499			
01324-013	1000	113	2.000			
01324-023	2000	226	2.749			
01324-053	5000	565	3.000	3/8"	C.W. UPSCALE	
01324-014	10000	1130	3.749			
01324-153	15000	1700	4.000			
01324-024	20000	2260	4.749			

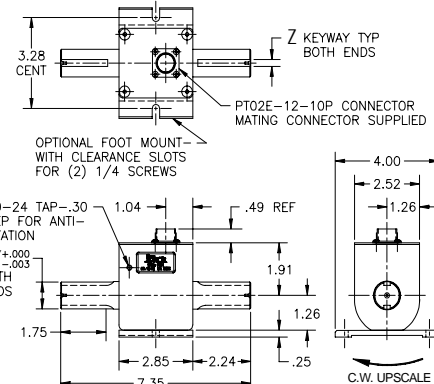
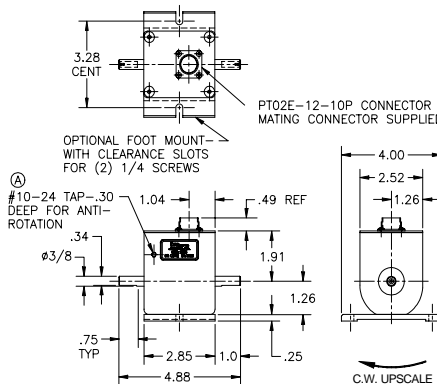


Figure C.4: Snapshot of torque sensor mfr. datasheet. Part number is 01324-052.

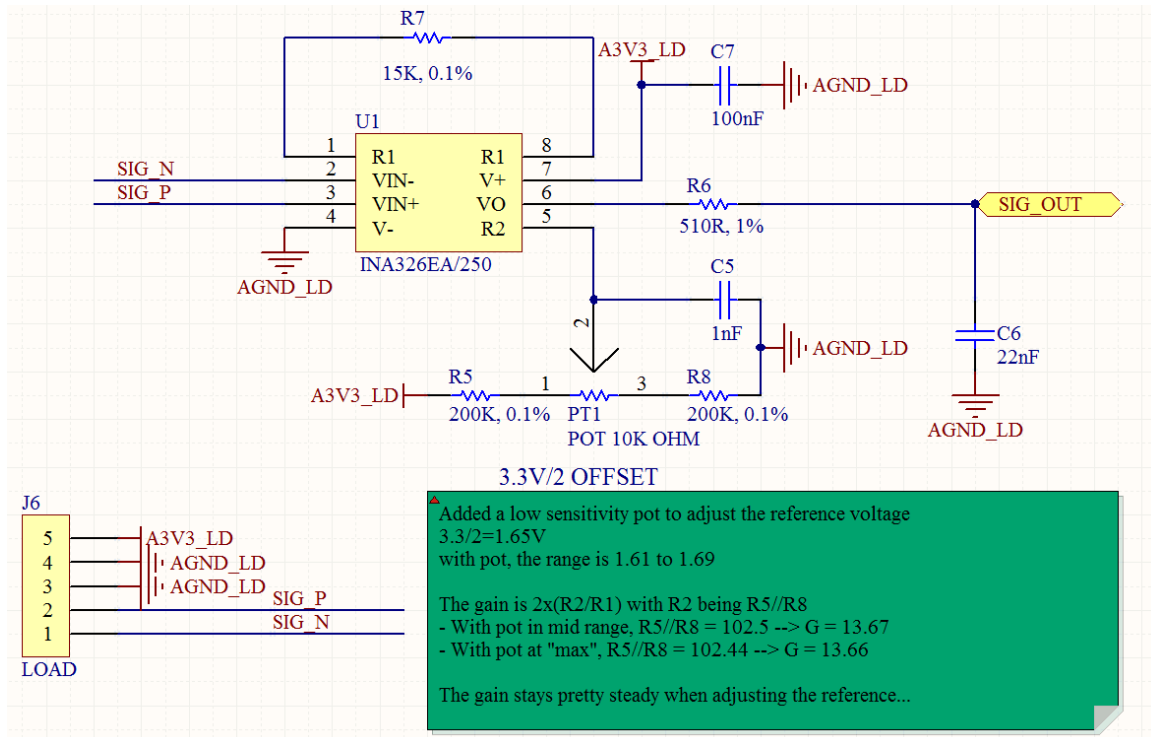


Figure C.5: Torque sensor op-amp circuit on M3\_LOADX3 board. Both the torque sensor and op-amp have a positive excitation voltage of 3.3V and negative excitation voltage of zero (ground). There is a hardware offset of 1.65V. The op-amp gain was originally set to around 13.66 but was probably increased by Meka due to very low load cell output voltage. The microcontroller reading the torque sensor output has a 12-bit ADC resolution and values are passed from the microcontroller to the EtherCAT bus without conversions.



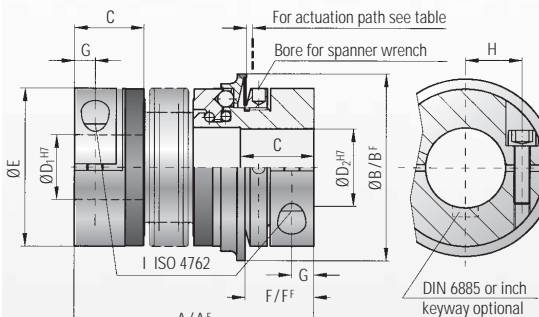
single-position  
multi-position  
load holding  
full disengagement



## MODEL SK2

**BACKLASH FREE TORQUE LIMITER**

with clamping hub



Optional sealed version for wash down and food service application. See page 16.

**Material:**  
Bellows made of highly elastic stainless steel  
Torque limiter: High strength hardened steel  
Hub material: up to series 80 aluminium from series up 150 steel

**Design:**  
With a single radial clamping screw per hub

**Temperature range:**  
-30° C to +110° C

**Backlash:**  
Absolutely backlash free as a result of the frictional clamp connection and the patented R+W principle

**Service life:**  
These coupling are maintenance free and have extreme service life as long as the performance limits are not exceeded.

**Fit tolerance:**  
Tolerance between hub and shaft 0.01-0.05 mm

**Ordering specifications:**  
see page 11

Model SK 2	Series																											
	1.5	2	4.5	10	15	30	60	80	150	200	300	500	800	1500														
Adjustment range available from - to (approx. values) (Nm)	$T_{KN}$ 0.1-0.6 0.4-1 0.8-1.5	0.2-1.5 or 0.5-2	1-3 or 3-6	2-6 or 8-20	5-10 or 8-20	10-25 or 20-40	10-30 or 25-80	20-70 or 30-90	20-70 or 45-150 80-180	30-90 60-160 120-240	100-200 150-240 200-320	80-200 200-350 300-500	400-650 500-800 650-950	650-800 700-1200 1000-1800														
Adjustment range available from - to (approx. values) (full disengagement) (Nm)	$T_{KN}$ 0.3-0.8 or 0.6-1.3	0.5-2	2.5-4.5	2-5 or 5-10	7-15	8-20 or 16-30	20-40 or 30-60	20-60 or 40-80 80-150	20-60 40-80 80-150	80-140 120-180 160-300	120-180 60-150 160-200	100-150 100-300 160-300	200-400 200-500 450-800	1000-1250 1250-1500														
Overall length (mm)	$A$	42	46	51	57	65	65	74	75	82	87	95	102	112	115	127	116	128	128	140	139	153	163	177	190	223		
Overall length, (full disengagement) (mm)	$A^F$	42	46	51	57	65	65	74	75	82	87	95	102	112	117	129	118	130	131	143	142	156	167	181	201	232		
Actuation ring $\emptyset$ (mm)	$B$	23	29	35	45	55	65	73	92	92	99	120	135	152	174													
Actuation ring $\emptyset$ (full disengagement) (mm)	$B^F$	24	32	42	51.5	62	70	83	98	98	117	132	155	177	187													
Fit length (mm)	$C$	11	13	16	16	22	27	31	35	35	40	42	51	48	67													
Inner diameter from $\emptyset$ to $\emptyset$ H7 (mm)	$D_1/D_2$	3.8	4.12	5.14	6.20	10.26	12.30	15.32	19.42	19.42	24.45	30.60	35.60	40.75	50.80													
Outer diameter of coupling (mm)	$E$	19	25	32	40	49	55	66	81	81	90	110	123	134	157													
Distance (mm)	$F$	12	13	15	17	19	24	30	31	31	35	45	50	63														
Distance (full disengagement) (mm)	$F^F$	11.5	12	14	16	19	22	29	31	30	33	35	43	54	61													
Distance (mm)	$G$	3.5	4	5	5	6.5	7.5	9.5	11	11	12.5	13	17	18	22.5													
Distance between centers (mm)	$H$	6	8	10	15	17	19	23	27	27	31	39	41	2x48	2x55													
ISO 4762 screws	$I$	M2.5	M3	M4	M4	M5	M6	M8	M10	M10	M12	M12	M16	2xM16	2xM20													
Tightening torque (Nm)	$I$	1	2	4	4.5	8	15	40	50	70	120	130	200	250	300	420	83.0											
Approx. weight (kg)		0.035	0.07	0.2	0.3	0.4	0.6	1.0	2.0	2.4	4.0	5.9	9.6	14	21													
Moment of inertia ( $10^{-3}$ kgm <sup>2</sup> )	$J_{res}$	0.01	0.01	0.02	0.06	0.07	0.10	0.15	0.27	0.32	0.75	0.80	1.80	1.90	2.50	2.80	5.10	5.30	11.5	11.8	22.8	23.0	42.0	83.0				
Torsional stiffness ( $10^3$ Nm/rad)	$C_1$	0.7	1.2	1.3	7	5	9	8	20	15	39	28	76	55	129	85	175	110	191	140	420	350	510	500	780	1304		
Lateral misalignment max. (mm)		0.15	0.20	0.25	0.20	0.30	0.15	0.20	0.25	0.20	0.25	0.20	0.25	0.20	0.25	0.25	0.25	0.30	0.25	0.30	0.25	0.30	0.35	0.35	0.35			
Angular misalignment max. (degrees)		1	1	1.5	1.5	2	1.5	1	1.5	1	1.5	1	1.5	1	1.5	1	1.5	1.5	1.5	2	2	2.5	2.5	2.5	2.5			
Lateral spring stiffness (N/mm)		70	40	30	200	45	280	145	475	137	900	270	1200	420	920	255	1550	435	2040	610	3750	1050	2500	840	2000	3600		
Actuation path (mm)		0.7	0.8	0.8	1.2	1.5	1.5	1.7	1.9	1.9	2.2	2.2	2.2	2.2	2.2	2.2	2.2	2.2	2.2	2.2	2.2	2.2	2.2	2.2	3			

**A<sup>F</sup>, B<sup>F</sup>, F<sup>F</sup> = Full disengagement version**

(smaller sizes on request)

Figure C.6: Snapshot of torque limiter mfr. datasheet. Part number is SK260.

75

## Specifications:

- Diameter: 8 inches
- Width Across Middle: 1.05 inches
- Bore: 1.124 inch diameter bore
- Bolt Pattern: 6 hole 1.875" diameter bolt circle
- Body Material: 3 - 1/8" thick aluminum with aluminum omni spacer
- Load Capacity: 100 pounds
- Coefficient of Friction, Forward/Backwards: Static: 1, Dynamic: 0.8-0.88
- Coefficient of Friction, Sideways: Static: 0.2-0.27, Dynamic: 0.16-0.2
- Weight: 2.2 pounds
- Repairable by removing perimeter #10-32 screws and center #10-32 screws
- Number of Rollers: 36
- Roller Material: Black SBR Rubber
- Roller Bearing Material: Brass
- Roller Axle: Steel Dowel Pin
- Roller Diameter: 3/4 inch
- Roller Durometer: 80A

Figure C.7: Snapshot of omni wheel specifications from mfr. website. Part number is am-0559.



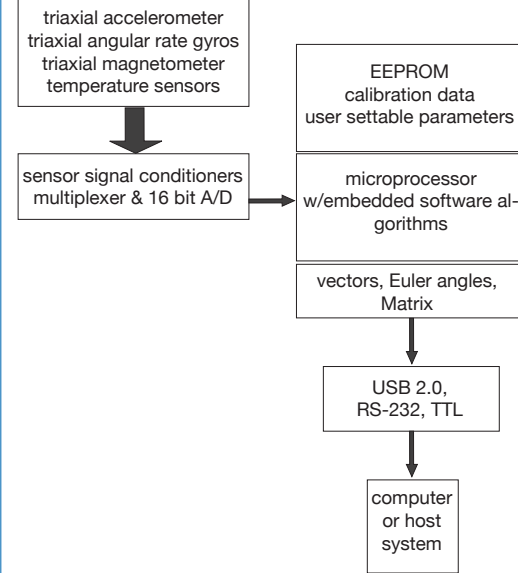
## Specifications

Orientation range	360° about all axes
Accelerometer range	± 5 g standard; ± 2 g, ± 18 g, and ± 50 g also available
Accelerometer bias stability	± 0.005 g for ± 5 g range ± 0.003 g for ± 2 g range ± 0.010 g for ± 18 g range ± 0.050 g for ± 50 g range
Accelerometer nonlinearity	0.2 %
Gyro range	± 300°/sec standard, ± 1200°/sec, ± 600°/sec, ± 150°/sec, ± 50°/sec also available
Gyro bias stability	± 0.2°/sec for ± 300°/sec
Gyro nonlinearity	0.2 %
Magnetometer range	± 2.5 Gauss
Magnetometer nonlinearity	0.4 %
Magnetometer bias stability	0.01 Gauss
A/D resolution	16 bits (SAR) (oversampled to 17 bits)
Orientation Accuracy	± 0.5° typical for static test conditions ± 2.0° typical for dynamic (cyclic) test conditions & for arbitrary orientation angles
Orientation resolution	<0.1°
Repeatability	0.2°
Output modes	acceleration, angular rate, and magnetic field deltaAngle and deltaVelocity Euler angles quaternion rotation matrix
Interface options	standard: USB 2.0 or RS232 OEM: USB 2.0 / TTL serial (3.3 volts)
Data rate	1 Hz to 1,000 Hz
Filtering	sensors sampled at 30 kHz, digitally filtered (user adjustable) and scaled into physical units; coning and sculling integrals computed at 1 kHz.
Baud rate	115,200 baud to 921,600 baud
Supply voltage	standard: 3.2 to 16 volts <sup>1</sup> OEM: 3.2 to 5.5 volts
Power consumption	80 mA @ 5 volts with USB
Connectors	micro-DB9, OEM: Samtec FTSH-105-01-F-D-K
Operating temp.	-40 °C to +70 °C (consult factory for higher temperature operation)
Dimensions	44 mm x 25 mm x 11 mm - excluding mounting tabs, width across tabs 37 mm, OEM: 38 mm x 24 mm x 12 mm
Weight	18 grams RS-232 and USB, 11.5 grams OEM
Shock limit	1000 g (unpowered), 500g (powered)

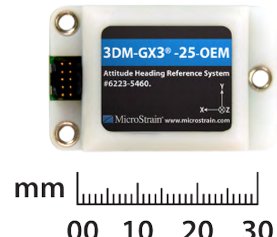
1. Applies to serial numbers 2290 and higher. See tech note TN-10023 for details of power supply operation, and for power supply voltage limits of earlier serial numbers.

\*Accuracy and stability specifications obtained over operating temperatures of -40 to 70°C with known sine and step inputs, including angular rates of ± 300° per second.

Copyright © 2011 MicroStrain Inc.  
MicroStrain, and 3DM-GX3 are trademarks of MicroStrain Inc.  
Specifications are subject to change without notice.  
Version # 1.07a



The system architecture has been carefully designed to substantially eliminate common sources of error such as hysteresis induced by temperature changes and sensitivity to supply voltage variations. On-board coning and sculling compensation allows for use of lower data output rates while maintaining performance of a fast internal sampling rate.



mm  
00 10 20 30

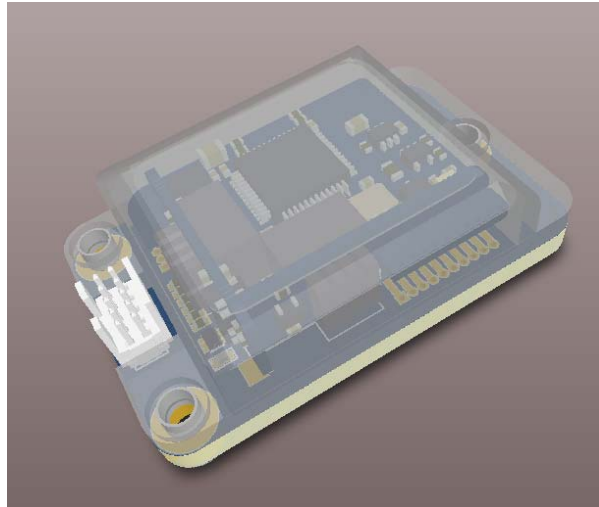
Weighing only 11.5 grams, the OEM version of the 3DM-GX3® -25 AHRS



Figure C.8: Snapshot of AHRS mfr. datasheet.

## 3DM-GX3-25 OEM Mounting Information

Preliminary 4/20/2009



### **Connector:**

The connector used on the 3DM-GX3-25 OEM module is a Samtec fine pitch (0.050") 5 x 2 (10 pin) keyed header connector. Cables are IDC ribbon cables. Connectors and cables in any length can be ordered directly from Samtec. Refer to the Samtec website for specific order information.

**Connector:** Samtec FTSH-105-01-F-D-K.

**Mates with** Samtec FFSD-05-D-xx.xx-01-N (where xx.xx is length of cable in inches)

### **Pinout:**

Pin	Name	Type	Description
1	USBDM	BiDir	USB D- Signal
2	USBDP	BiDir	USB D+ Signal
3	VBUS	Power	Power – Minimum 3.1 volts, Maximum 5.5 volts DC
4	UARTRX	Input	LVTTL (5V Tolerant) Serial UART receive (connect to host Transmit)
5	UARTTX	Output	LVTTL (5V Tolerant) Serial UART transmit (connect to host Receive)
6	NC		not connected
7	GPIO1	I/O	General purpose I/O
8	GND	Ground	Power and signal ground
9	GPIO2	I/O	General purpose I/O
10	nENABLE	Input	Module enable. LVTTL low enables. LVTTL high disables

Figure C.9: Snapshot of AHRS mounting information.

## Bibliography

- [1] T. Asfour, K. Regenstein, P. Azad, J. Schröder, A. Bierbaum, N. Vahrenkamp, and R. Dillmann. ARMAR-III: An Integrated Humanoid Platform for Sensory-Motor Control. In *IEEE-RAS 6th International Conference on Humanoid Robots*, pages 169–175, 2006.
- [2] Rainer Bischoff, Ulrich Huggenberger, and Erwin Prassler. KUKA youBot – a mobile manipulator for research and education. In *IEEE International Conference on Robotics and Automation*, pages 1–4, 2011.
- [3] Kyung-Seok Byun and Jae-Bok Song. Design and Construction of Continuous Alternate Wheels for an Omnidirectional Mobile Robot. *Journal of Robotic Systems*, 20(9):569–579, September 2003.
- [4] Peng Chen, Shinichiro Mitsutake, Takashi Isoda, and Tielin Shi. Omni-Directional Robot and Adaptive Control Method for Off-Road Running. *IEEE Transactions on Robotics and Automation*, 18(2):251–256, 2002.
- [5] Daisuke Chugo, Kuniaki Kawabata, Hayato Kaetsu, Hajime Asama, and Takeshi Mishima. Development of Omnidirectional Vehicle with Step-Climbing ability. In *2003 IEEE International Conference on Robotics and Automation (Cat. No.03CH37422)*, volume 3, pages 3849–3854, 2003.
- [6] Alexander Dietrich, Thomas Wimböck, and Alin Albu-Schäffer. Dynamic Whole-Body Mobile Manipulation with a Torque Controlled Humanoid Robot via Impedance Control Laws. In *IEEE/RSJ International Conference on Intelligent Robots and Systems*, pages 3199–3206, 2011.
- [7] Alexander Dietrich, Thomas Wimböck, Alin Albu-Schäffer, and Gerd Hirzinger. Singularity Avoidance for Nonholonomic, Omnidirectional Wheeled Mobile Platforms with Variable Footprint. In *IEEE International Conference on Robotics and Automation*, pages 6136–6142, 2011.
- [8] Tiago P. do Nascimento, Augusto Loureiro da Costa, and Cristiane Correia Paim. AxeBot Robot: The Mechanical Design for an Autonomous Omnidirectional Mobile Robot. In *Electronics, Robotics and Automotive Mechanics Conference (CERMA)*, pages 187–192, 2009.

- [9] Aaron Ladd Edsinger. *Robot Manipulation in Human Environments*. PhD thesis, Massachusetts Institute of Technology, 2007.
- [10] L. Ferrière, B. Raucent, and G. Campion. Design of Omnimobile Robot Wheels. In *IEEE International Conference on Robotics and Automation*, volume 4, pages 3664–3670, 1996.
- [11] Julien Frémy, François Michaud, and Michel Lauria. Pushing a Robot Along - A Natural Interface for Human-Robot Interaction. In *IEEE International Conference on Robotics and Automation*, pages 3440–3445, 2010.
- [12] M. Fuchs, C. Borst, P.R. Giordano, A. Baumann, E. Kraemer, J. Langwald, R. Gruber, N. Seitz, G. Plank, K. Kunze, R. Burger, F. Schmidt, T. Wimboeck, and G. Hirzinger. Rollin’ Justin - Design considerations and realization of a mobile platform for a humanoid upper body. In *IEEE International Conference on Robotics and Automation*, pages 4131–4137, 2009.
- [13] Elena Garcia, Maria Antonia Jimenez, Pablo Gonzalez-de-Santos, and Miguel Armada. The Evolution of Robotics Research: From Industrial Robotics to Field and Service Robotics. *IEEE Robotics and Automation Magazine*, 14(1):90–103, 2007.
- [14] Robert Holmberg. *Design and Development of Powered-Caster Holonomic Mobile Robots*. PhD thesis, Stanford University, 2000.
- [15] Robert Holmberg and Oussama Khatib. Development and Control of a Holonomic Mobile Robot for Mobile Manipulation Tasks. *The International Journal of Robotics Research*, 19(11):1066–1074, November 2000.
- [16] Tatsuzo Ishida and Atsuo Takanishi. A Robot Actuator Development With High Backdrivability. In *IEEE Conference on Robotics, Automation and Mechatronics*, pages 1–6, 2006.
- [17] Genya Ishigami, Elvine Pineda, Jim Overholt, Greg Hudas, and Karl Iagnemma. Performance Analysis and Odometry Improvement of an Omnidirectional Mobile Robot for Outdoor Terrain. In *IEEE/RSJ International Conference on Intelligent Robots and Systems*, pages 4091–4096, 2011.
- [18] Advait Jain and Charles C. Kemp. Pulling Open Doors and Drawers: Coordinating an Omni-directional Base and a Compliant Arm with Equilibrium Point Control. In *IEEE International Conference on Robotics and Automation*, pages 1807–1814, 2010.

- [19] Dirk Jansen and Holger Büttner. Real-time Ethernet: the EtherCAT solution. *Computing and Control Engineering*, 15(1):16–21, 2004.
- [20] Urs Kafader. *The selection of high-precision microdrives.* maxon academy, 2006.
- [21] O. Khatib, K. Yokoi, K. Chang, D. Ruspini, R. Holmberg, and A. Casal. Vehicle/Arm Coordination and Multiple Mobile Manipulator Decentralized Cooperation. In *IEEE/RSJ International Conference on Intelligent Robots and Systems*, pages 546–553, 1996.
- [22] Oussama Khatib. A Unified Approach for Motion and Force Control of Robot Manipulators: The Operational Space Formulation. *IEEE Journal of Robotics and Automation*, 3(1):43–53, 1987.
- [23] Masaaki Kumagai and Takaya Ochiai. Development of a robot balancing on a ball. In *International Conference on Control, Automation and Systems*, pages 433–438, October 2008.
- [24] M. Lauria, M.-A. Legault, M.-A. Lavoie, and F. Michaud. Differential Elastic Actuator for Robotic Interaction Tasks. In *IEEE International Conference on Robotics and Automation*, pages 3606–3611, May 2008.
- [25] T. B. Lauwers, G. A. Kantor, and R. L. Hollis. A Dynamically Stable Single-Wheeled Mobile Robot with Inverse Mouse-Ball Drive. In *IEEE International Conference on Robotics and Automation*, pages 2884–2889, 2006.
- [26] Tom Lauwers, George Kantor, and Ralph Hollis. One is Enough! In *Springer Tracts in Advanced Robotics*, pages 327–336. 2007.
- [27] Aaron Morris, Raghavendra Donamukkala, Anuj Kapuria, Aaron Steinfeld, Judith T. Matthews, Jacqueline Dunbar-Jacob, and Sebastian Thrun. A Robotic Walker That Provides Guidance. In *IEEE International Conference on Robotics and Automation*, volume 1, pages 25–30, 2003.
- [28] Gilles Mouroux, Cyril Novales, Gérard Poisson, and Pierre Vieuxres. Omnidirectional robot with spherical orthogonal wheels: concepts and analyses. In *IEEE International Conference on Robotics and Automation*, volume 2, pages 3374–3379, 2006.
- [29] Umashankar Nagarajan, Anish Mampetta, George A. Kantor, and Ralph L. Hollis. State transition, balancing, station keeping, and yaw control for a dynamically stable single spherical wheel mobile robot. In *IEEE International Conference on Robotics and Automation*, volume 2, pages 998–1003, 2009.

- [30] Roland Philippsen, Luis Sentis, and Oussama Khatib. An Open Source Extensible Software Package to Create Whole-Body Compliant Skills in Personal Mobile Manipulators. In *IEEE/RSJ International Conference on Intelligent Robots and Systems*, pages 1036–1041, 2011.
- [31] François G. Pin and Stephen M. Killough. A New Family of Omnidirectional and Holonomic Wheeled Platforms for Mobile Robots. *IEEE Transactions on Robotics and Automation*, 10(4):480–489, 1994.
- [32] Luis Sentis. *Synthesis and Control of Whole-Body Behaviors in Humanoid Systems*. PhD thesis, Stanford University, 2007.
- [33] Luis Sentis, Jaeheung Park, and Oussama Khatib. Compliant Control of Multi-contact and Center-of-Mass Behaviors in Humanoid Robots. *IEEE Transactions on Robotics*, 26(3):483–501, June 2010.
- [34] Sarmad Shams, Dongik Shin, Jungsoo Han, Ji Yeong Lee, Kyoosik Shin, and Chang-Soo Han. Compact Design of a Torque Sensor using Optical Technique and its Fabrication for Wearable and Quadruped Robots. In *IEEE/RSJ International Conference on Intelligent Robots and Systems*, pages 5127–5132, 2011.
- [35] Jae-Bok Song and Kyung-Seok Byun. Design and Control of a Four-Wheeled Omnidirectional Mobile Robot with Steerable Omnidirectional Wheels. *Journal of Robotic Systems*, 21(4):193–208, 2004.
- [36] Matthew Spenko, Haoyong Yu, and Steven Dubowsky. Robotic Personal Aids for Mobility and Monitoring for the Elderly. *IEEE Transactions on Neural Systems and Rehabilitation Engineering*, 14(3):344–51, September 2006.
- [37] Rob P. A. van Haendel. Design of an omnidirectional universal mobile platform. Technical report, Eindhoven University of Technology, 2005.
- [38] J. A. Vázquez and M. Velasco-Villa. Computed-Torque Control of an Omnidirectional Mobile Robot. In *4th International Conference on Electrical and Electronics Engineering*, pages 274–277, 2007.
- [39] Dieter Vischer and Oussama Khatib. Design and Development of High-Performance Torque-Controlled Joints. *IEEE Transactions on Robotics and Automation*, 11(4):537–544, 1995.
- [40] Masayoshi Wada and Shunji Mori. Holonomic and Omnidirectional Vehicle with Conventional Tires. In *IEEE International Conference on Robotics and Automation*, volume 4, pages 3671–3676, 1996.

- [41] Mark West and Haruhiko Asada. Design and Control of Ball Wheel Omnidirectional Vehicles. In *IEEE International Conference on Robotics and Automation*, pages 1931–1938, 1995.
- [42] Alexander N. Wilhelm. Design of a Mobile Robotic Platform with Variable Footprint. Master’s thesis, University of Waterloo, 2007.
- [43] David Williams and Oussama Khatib. The virtual linkage: a model for internal forces in multi-grasp manipulation. In *IEEE International Conference on Robotics and Automation*, pages 1025–1030. IEEE Comput. Soc. Press, 1993.
- [44] James H. Williams. *Fundamentals of Applied Dynamics*. John Wiley & Sons, Inc., New York, 1996.
- [45] Matthew M. Williamson. Series elastic actuators. Master’s thesis, Massachusetts Institute of Technology, 1995.
- [46] Haoyong Yu, Matthew Spenko, and Steven Dubowsky. Omni-Directional Mobility Using Active Split Offset Castors. *Journal of Mechanical Design*, 126(5):822–829, 2004.
- [47] Michael Zinn, Oussama Khatib, Bernard Roth, and J. Kenneth Salisbury. Playing It Safe: A New Actuation Concept for Human-Friendly Robot Design. *IEEE Robotics and Automation Magazine*, 11(2):12–21, January 2004.